



## Article

# Evaluation of 10-Year NOAA/NASA Suomi NPP and NOAA-20 VIIRS Reflective Solar Band (RSB) Sensor Data Records (SDR) over Deep Convective Clouds

Wenhui Wang <sup>1,\*</sup> , Changyong Cao <sup>2</sup> , Xi Shao <sup>1</sup>, Slawomir Blonski <sup>3</sup> , Taeyoung Choi <sup>3</sup>, Sirish Uprety <sup>1</sup>, Bin Zhang <sup>1</sup> and Yan Bai <sup>1</sup>

<sup>1</sup> CISESS/ESSIC, University of Maryland, College Park, MD 20740, USA; xi.shao@noaa.gov (X.S.); sirish.uprety@noaa.gov (S.U.); bin.zhang@noaa.gov (B.Z.); yan.bai@noaa.gov (Y.B.)

<sup>2</sup> NOAA/NESDIS/Center for Satellite Applications and Research, College Park, MD 20740, USA; changyong.cao@noaa.gov

<sup>3</sup> Global Science and Technology, Inc., Greenbelt, MD 20770, USA; slawomir.blonski@noaa.gov (S.B.); taeyoung.choi@noaa.gov (T.C.)

\* Correspondence: wenhui.wang@noaa.gov; Tel.: +1-301-683-3531

**Abstract:** The Visible Infrared Imaging Radiometer Suite (VIIRS) is a key instrument onboard the Suomi NPP (S-NPP) and the NOAA-20 satellites that provides state-of-the-art Earth observations for ocean, land, aerosol, and cloud applications. VIIRS Reflective Solar Band (RSB) Sensor Data Records (SDR, or Level 1b products) are calibrated and produced independently by The National Oceanic and Atmospheric Administration (NOAA) and the National Aeronautics and Space Administration (NASA) VIIRS science teams. Multiple versions of S-NPP and NOAA-20 VIIRS SDRs are available to date. This study evaluates the long-term calibration stability, biases, and inter-channel consistency of S-NPP and NOAA-20 VIIRS SDRs generated by NOAA and NASA over Deep Convective Clouds (DCC) to support downstream applications, especially climate data record studies. Five VIIRS RSB SDRs were analyzed in this study: (1) NOAA version 2 S-NPP VIIRS reprocessed SDRs (NOAA-NPP-V2, 2012–2020), (2) NASA Collection 1 S-NPP VIIRS SDRs (NASA-NPP-C1, 2012–2021), (3) NASA Collection 2 S-NPP VIIRS SDRs (NASA-NPP-C2, 2012–2021), (4) NOAA constant F-factor calibrated NOAA-20 VIIRS SDRs (NOAA-N20-ConstF, 2018–2021), and (5) NASA Collection 2 NOAA-20 VIIRS SDRs (NASA-N20-C2, 2018–2021). The DCC time series analysis results indicate that the calibrations of the three S-NPP VIIRS RSB SDRs are generally stable, with trends within  $\pm 0.1\%$ /year for all RSBs, except for M3–M4 (all three S-NPP SDRs) and I3 (NASA-NPP-C1 only). The calibration of NASA-NPP-C2 SDRs is more uniform at individual detector levels. NOAA-NPP-V2 and NASA-NPP-C1 SDRs exhibit non-negligible time-dependent detector level degradation in M1–M4 (up to 1.5% in 2020–2021), causing striping in the SDR imagery. The biases between NOAA and NASA S-NPP VIIRS RSB SDRs are from 0.1% to 2.4%. The calibrations of the two NOAA-20 VIIRS RSB SDRs are also generally stable, with trends within  $\pm 0.16\%$ /year. Small downward trends were observed in the visible and near-infrared (VIS/NIR) bands, and small upward trends were observed in the shortwave infrared (SWIR) bands for both NOAA and NASA NOAA-20 SDRs. The biases between NOAA and NASA NOAA-20 VIIRS RSB SDRs are nearly constant over time and within  $\pm 0.2\%$  for VIS/NIR bands and  $\pm 0.7\%$  for SWIR bands. There exists large inter-satellite biases between S-NPP and NOAA-20 VIIRS SDRs, especially in the VIS/NIR bands (up to 4.5% for NOAA SDRs and up to 7% for NASA SDRs). In addition, the DCC reflectance of S-NPP VIIRS RSB spectral bands is more consistent with that of the SCanning Imaging Absorption SpectroMeter for Atmospheric CHartography (SCIAMACHY) than that of NOAA-20. Bands M4 and M9 seem out of family in all five S-NPP and NOAA-20 RSB SDRs evaluated.

**Keywords:** Visible Infrared Imaging Radiometer Suite (VIIRS); Suomi NPP (S-NPP); NOAA-20; Deep Convective Clouds (DCC); Reflective Solar Bands (RSB); Sensor Data Records (SDR); level 1b (L1B) products; calibration stability and biases; inter-satellite biases; inter-channel calibration consistency



**Citation:** Wang, W.; Cao, C.; Shao, X.; Blonski, S.; Choi, T.; Uprety, S.; Zhang, B.; Bai, Y. Evaluation of 10-Year NOAA/NASA Suomi NPP and NOAA-20 VIIRS Reflective Solar Band (RSB) Sensor Data Records (SDR) over Deep Convective Clouds. *Remote Sens.* **2022**, *14*, 3566. <https://doi.org/10.3390/rs14153566>

Academic Editor: Nicola Pergola

Received: 4 May 2022

Accepted: 18 July 2022

Published: 25 July 2022

**Publisher's Note:** MDPI stays neutral with regard to jurisdictional claims in published maps and institutional affiliations.



**Copyright:** © 2022 by the authors. Licensee MDPI, Basel, Switzerland. This article is an open access article distributed under the terms and conditions of the Creative Commons Attribution (CC BY) license (<https://creativecommons.org/licenses/by/4.0/>).

## 1. Introduction

The Visible Infrared Imaging Radiometer Suite (VIIRS) is a key instrument onboard the Suomi NPP (S-NPP) and the National Oceanic and Atmospheric Administration-20 (NOAA-20) satellites. VIIRS has 14 Reflective Solar Bands (RSB), 7 Thermal Emissive Bands, and 1 Day–Night Band, covering a spectrum range from 0.41 to 12  $\mu\text{m}$ . With strong heritages from the Moderate-Resolution Imaging Spectroradiometer (MODIS) and the Advanced Very-High-Resolution Radiometer (AVHRR), VIIRS RSB Sensor Data Records (SDRs, or level 1b products) are used for a wide variety of environmental and climate data records, such as cloud and aerosol properties, ocean color, vegetation indices, and surface reflectance/albedo.

The on-orbit calibration of VIIRS RSBs is complex, primarily depending on the onboard Solar Diffuser (SD) and Solar Diffuser Stability Monitor (SDSM) [1,2]. VIIRS RSB on-orbit calibration factors (F-factors) are derived using SD observations when the SD is fully illuminated by the Sun over the Antarctic region. Due to solar exposure, SD degrades over time, especially in shorter wavelengths. The degradation of SD is estimated and corrected using the ratio of SDSM observations in the SD view and solar view. Due to the uncertainties in on-orbit calibrations, the calibration accuracy, stability, and relative bias of the NOAA-20 and S-NPP VIIRS reflectance are continuously evaluated using vicarious methods over stable targets, such as the Moon, deserts, and Deep Convective Clouds (DCC), to ensure high-quality RSB SDRs for data users. Vicarious calibration results from the lunar and DCC trendings are also used in the decision making of operational calibration updates [3,4] and in the recalibration analyses [5]. To address inconsistencies due to the calibration algorithm and parameter updates over time and to mitigate residual degradations in the operational processing, S-NPP and NOAA-20 VIIRS SDRs have been reprocessed to support downstream applications. Multiple versions of S-NPP and NOAA-20 VIIRS SDRs, calibrated and produced independently by NOAA and the National Aeronautics and Space Administration (NASA) teams, are available to downstream data users (see Section 2). However, limited evaluation results are available so far.

The purpose of this study is to evaluate the long-term calibration stability, bias, and inter-channel calibration consistency of the reprocessed VIIRS RSB SDRs using the DCC methods. DCCs are stable Earth targets, and the DCC methods have widely been used for the on-orbit calibration stability monitoring of satellite radiometers in the solar reflective spectrum [4,6–14]. In this study, we also used DCCs to evaluate the biases between NOAA-20 and S-NPP VIIRS SDRs, SDRs calibrated by different science teams, and the inter-channel calibration consistency. Ten years (2012–2021) of S-NPP VIIRS RSB SDRs were analyzed; four years (2018–2021) of NOAA-20 VIIRS SDR data were analyzed. The results from this study are useful for supporting downstream climate and environmental data record studies. This paper is organized as follows. Section 2 introduces the S-NPP and NOAA-20 VIIRS SDRs evaluated in this study. Section 3 presents the DCC methods for VIIRS. The results are discussed in Section 4. Section 5 summarizes this study.

## 2. S-NPP and NOAA-20 VIIRS SDRs

VIIRS has 14 RSBs, including 9 visible near-infrared (VIS/NIR, M1–M7, and I1–I2) and 5 short-wave infrared (SWIR, M8–M11, and I3) bands. VIIRS M1–M5 and M7 are the dual-gain bands, while M6, M8–M11, and I1–I3 are single-gain bands. M1–M11 are moderate-resolution bands (M-bands, 750 m at nadir); I1–I3 are imagery resolution bands (I-bands, 375 m at nadir). There are 16 M-band detectors and 32 I-band detectors. The spatial and spectral characteristics of VIIRS RSBs, including spatial resolution, center wavelength, gain stage, typical radiance ( $L_{typ}$ ), minimum radiance ( $L_{min}$ ), and maximum radiance ( $L_{max}$ ) specifications, are summarized in Table 1.

NOAA-20 and S-NPP VIIRS SDRs are independently calibrated and produced by the NOAA and NASA teams. The NOAA VIIRS SDRs are calibrated by the NOAA STAR VIIRS radiance team, while the NASA VIIRS SDRs are calibrated by the NASA VIIRS Calibration Support Team (VCST). In addition, VIIRS RSB SDRs are also calibrated by the NOAA and

NASA ocean color teams for ocean color applications [15–22]. During the past 10 years, extensive efforts have been made to recalibrate/reprocess S-NPP and NOAA-20 VIIRS RSB SDRs to generate consistent data records for downstream applications [5,18,19,22–26]. In this study, five reprocessed VIIRS SDR products, calibrated by the NOAA and NASA VIIRS radiance science teams, were analyzed: (1) NOAA STAR S-NPP version 2 reprocessed VIIRS SDRs, (2) NASA Collection-1 S-NPP VIIRS SDRs, (3) NASA Collection-2 S-NPP VIIRS SDRs, (4) NOAA STAR constant F-factors calibrated NOAA-20 VIIRS SDRs, and (5) NASA Collection 2 NOAA-20 VIIRS SDRs. These five datasets are summarized in Table 2. VIIRS RSB SDRs are calibrated independently by the NOAA and NASA VIIRS science teams using different methodologies, which may result in differences in the NOAA and NASA VIIRS SDRs.

Besides the five reprocessed VIIRS SDRs, NOAA operational (near real-time) SDRs for S-NPP (NOAA-NPP-OPR, 2012–2021) and NOAA-20 (NOAA-N20-OPR, 2018–2021) were also used in this study. Note that there exist significant inconsistencies in the NOAA operational VIIRS SDRs due to the calibration algorithm/parameter updates over time, especially during the early missions [5,11,27,28]. Therefore, the two NOAA operational SDRs were used for comparison purposes only. It is not recommended to use them for long-term environment and climate data record studies.

**Table 1.** Spatial and spectral characteristics of NOAA-20 and S-NPP VIIRS RSBs. The unit of  $L_{typ}$  (typical radiance),  $L_{min}$  (minimum radiance), and  $L_{max}$  (maximum radiance) is  $W/(m^2 \cdot \mu m \cdot sr)$ . M1–M5 and M7 are dual-gain bands: H (high-gain) and L (low-gain) I1–I3, M6, and M8–M11 are single-gain bands (S).

|         | Spatial Resolution at Nadir (m) | Center Wavelength ( $\mu m$ ) |         | Gain  | $L_{typ}$ | $L_{min}$                  | $L_{max}$ |      |
|---------|---------------------------------|-------------------------------|---------|-------|-----------|----------------------------|-----------|------|
|         |                                 | S-NPP                         | NOAA-20 |       |           |                            |           |      |
| VIS/NIR | M1                              | 750                           | 0.411   | 0.412 | H         | 44.9                       | 30        | 135  |
|         |                                 |                               |         |       | L         | 155                        | 615       |      |
|         | M2                              | 750                           | 0.444   | 0.445 | H         | 40                         | 26        | 127  |
|         |                                 |                               |         |       | L         | 146                        | 687       |      |
|         | M3                              | 750                           | 0.486   | 0.489 | H         | 32                         | 22        | 107  |
|         |                                 |                               |         |       | L         | 123                        | 702       |      |
|         | M4                              | 750                           | 0.551   | 0.557 | H         | 21                         | 12        | 78   |
|         |                                 |                               |         |       | L         | 90                         | 667       |      |
|         | I1                              | 375                           | 0.639   | 0.644 | S         | 22                         | 22        | 718  |
|         | M5                              | 750                           | 0.672   | 0.667 | H         | 10                         | 9         | 59   |
|         |                                 |                               |         |       | L         | 68                         | 651       |      |
| M6      | 750                             | 0.745                         | 0.746   | S     | 9.6       | 5.3                        | 41        |      |
| I2      | 375                             | 0.862                         | 0.867   | S     | 25        | 25                         | 349       |      |
| M7      | 750                             | 0.862                         | 0.868   | H     | 6.4       | 3.4                        | 29        |      |
|         |                                 |                               |         | L     | 33.4      | 349                        |           |      |
| M8      | 750                             | 1.238                         | 1.238   | S     | 5.4       | 3.5                        | 165       |      |
| M9      | 750                             | 1.375                         | 1.375   | S     | 6         | 0.6                        | 77.1      |      |
| SWIR    | I3                              | 375                           | 1.602   | 1.604 | S         | 7.3                        | 7.3       | 72.5 |
|         | M10                             | 750                           | 1.602   | 1.605 | S         | 7.3                        | 1.2       | 71.2 |
|         | M11                             | 750                           | 2.257   | 2.258 | S         | 0.12(NPP)<br>0.1 (NOAA-20) | 0.12      | 31.8 |

**Table 2.** S-NPP and NOAA-20 VIIRS RSB SDRs evaluated in this study.

|         | Name            | Time Period | Note  |
|---------|-----------------|-------------|---|
| S-NPP   | NOAA-NPP-V2     | 2012–2020   | NOAA Version 2 Reprocessed S-NPP VIIRS SDRs.          |
|         | NASA-NPP-C1     | 2012–2021   | NASA Collection 1.0 SIPS S-NPP VIIRS level 1B data.   |
|         | NASA-NPP-C2     | 2012–2021   | NASA Collection 2.0 SIPS S-NPP VIIRS level 1B data.   |
| NOAA-20 | NOAA-N20-ConstF | 2018–2021   | NOAA constant F-factor calibrated NOAA-20 VIIRS SDRs. |
|         | NASA-N20-C2     | 2018–2021   | NASA Collection 2.0 SIPS NOAA-20 VIIRS level 1B data. |

### 2.1. S-NPP VIIRS RSB SDRs

S-NPP VIIRS was launched on 28 October 2011, with the nadir door opened on 21 November 2011, cryoradiator door opened on 20 January 2012, and cold focal plane assemblies reaching the nominal temperature on 22 January 2012. S-NPP VIIRS RSBs have experienced significant on-orbit degradations due to tungsten oxide contamination on the RTA mirrors [2], especially in the M7–M8 wavelengths, which showed degradations ~60% since launch by the end of 2021 [29]. Ten years of S-NPP VIIRS SDRs (from February 2012 to December 2021) generated by NOAA and NASA were analyzed and compared in this study.

The NOAA S-NPP VIIRS SDRs evaluated in this study are the version 2 reprocessed data (NOAA-NPP-V2) [5,24]. Nine years of NOAA-NPP-V2 data records (2012–2020) are available to date. The calibration methodologies for NOAA-NPP-V2 RSBs are well-described in a previous study [5]. The NOAA-NPP-V2 dataset originally covers a time period from launch to February 2017. It was recently extended to December 2020, calibrated using the same methodologies. The 2021 data has not been reprocessed yet; therefore, they were not considered here. The consistent Thuillier solar irradiance model [30] was used for the entire NOAA-NPP-V2 data record. The long-term calibration stability of the VIS/NIR bands was improved using a Kalman filter-based approach that incorporates calibration results from on-board solar calibrations [31], lunar calibrations [32], desert sites [33], VIIRS-MODIS SNOs [34], and DCCs [4,11]. For the VIS/NIR bands, the SD degradation factors (H-factor) were derived using an automatic calibration procedure (RSBAutoCal) and the latest calibration parameters that are currently used by NOAA operational processing [4,31]. A SD Surface Roughness Rayleigh Scattering model was used to account for the SD degradation in the SWIR bands [35]. Two versions (the prelaunch and the 5 April 2013 versions) of relative response functions (RSR) were used to account for the on-orbit changes caused by the different rates of degradation of the VIIRS optical components (especially RTA) at different wavelengths. In addition, the 24 February 2019 SD measurement anomaly was resolved by applying the updated SD degradation factors for the SWIR bands [36]. The 16 to 17 January 2020 RSB anomaly due to solar vector error was fixed by applying the updated ephemeris look-up table (LUT) [37]. Five years of NOAA-NPP-V2 data (from February 2012 to February 2017) were evaluated using a monthly DCC time series [5]. In this study, nine years of data were analyzed and compared with the S-NPP VIIRS RSB SDRs produced by NASA.

Two versions of the NASA S-NPP VIIRS SDRs were evaluated: (1) NASA-NPP-C1 and (2) NASA-NPP-C2. Both versions are calibrated by the NASA VCST and produced by the NASA Land Science Investigator-led Processing System (SIPS). The on-orbit radiometric calibration algorithms for NASA-NPP-C1 are given by [26,38–41]. The MODTRAN 4.3 solar irradiance model is used for both NASA S-NPP VIIRS RSB SDRs. Time-dependent (or modulated) RSRs were derived and used to account for the on-orbit changes caused by the different rates of degradation of the VIIRS optical components at different wavelengths. Improved SD degradation factors (H-factor) and F-factors were developed using the yaw maneuver data and regular SDSM on-orbit calibration data. H-factors at the SWIR wavelengths were determined using a wavelength power law. The annual undulation of F-factors was corrected by accounting for the solar angle dependences of the H-factors. The performances of NASA-NPP-C1 VIIRS RSB TOA reflectance were evaluated over the Libya-4 desert sites by comparing them with the

NASA NOAA-20 VIIRS Collection-2 (see Section 2.2) data and the matching MODIS bands (Collection 6.1) [25]. The calibration algorithms used for NASA-NPP-C2 RSB SDRs are similar to those used in NASA-NPP-C1. The major improvements in NASA-NPP-C2 include the removal of image striping caused by nonuniform degradation of the SD [13,42,43], improvements to the method for combining lunar and SD data, the mitigation of the 24 February 2019 SD measurements anomaly, and the estimation of the SD degradation in the SWIR spectrum and fitting strategy improvements for look-up table delivery [23].

## 2.2. NOAA-20 VIIRS RSB SDRs

NOAA-20 VIIRS was launched on 18 November 2017. Its nadir door was opened on 13 December 2017, cryoradiator door was opened on 3 January 2018, and cold focal plane assemblies reached the nominal temperature on 5 January 2018. Four years (6 January 2018 to 5 January 2022) of NOAA-20 VIIRS RSB SDRs, generated by the NOAA and NASA teams, are analyzed in this paper. Different from S-NPP, the on-orbit instrument responsivity degradations of NOAA-20 VIIRS RSBs have been very small based on various vicarious trending results, including lunar calibrations [3,20,44–46] and daily DCC time series [3,4].

The NOAA generated NOAA-20 VIIRS RSB SDRs (NOAA-N20–constant F) consist of 4 months of reprocessed SDRs during the beginning of the mission and 3 years and 2 months of operational data. The SDRs from 6 January 2018 to 4 November 2021 were calibrated using consistent constant F-factors, which were derived from the improved F-factors during the early mission, which were updated using H-factors derived by the improved SDSM sun screen transmittance function combining yaw maneuver data and on-orbit SDSM datasets [3]. Small upward trends were introduced to the F-factors used in the NOAA operational processing since 4 November 2021 to mitigate the recently observed slow degradations in the NOAA-20 VIIRS VIS/NIR bands [47]. In this study, only 2 months of data were calibrated using the updated F-factors, and the impacts of this update can be ignored (less than 0.02% or 0.005%/year). Note that the entire NOAA-N20-ConstF SWIR bands data records are calibrated using constant F-factors.

NASA Collection 2 NOAA-20 VIIRS SDRs (NASA-N20-C2) were also evaluated in this paper. The RSB calibration algorithms for NASA-N20-C2 are described in [46,48,49]. Improved H-factors (for the SDSM view) were used in the calibrations by using SD and SDSM attenuation screen transmittance functions obtained by using calibration data collected during both the yaw maneuver and a small portion of regular orbits. Moreover, the H-factor for the RTA view, which was derived from the H-factor for the SDSM view and the S-NPP VIIRS results, was used in the calibrations.

## 3. The Monthly and Daily DCC Methods for VIIRS

DCCs are extremely cold clouds over the Inter-Tropical Convergence Zone (ITCZ). They are stable Earth targets with near-Lambertian reflectance and can be identified using a single thermal band centered at  $\sim 11 \mu\text{m}$  (VIIRS M15). The DCC technique has widely been used for on-orbit calibration stability monitoring of satellite radiometers in the solar reflective spectrum [4,7–11,14,50,51]. It is a statistical-based method. Traditionally, monthly DCC mode time series are used for VIS/NIR individual band calibration stability analyses, and the mean time series are used for SWIR individual band stability analyses. Moreover, DCC mean ratio time series are also used for inter-satellite bias study. Besides the traditional monthly DCC time series, daily DCC time series that use daily DCC statistics were also developed for VIIRS operational calibration monitoring and re-calibration analyses [4,52]. The trend derived using daily DCC time series is similar to the monthly DCC time series, while the uncertainty of the trends is smaller due to the higher temporal resolution. It is more suitable for trending relatively short time series, such as for NOAA-20 VIIRS RSB SDRs. The same DCC identification criteria are used for the daily and monthly DCC methods for VIIRS. These criteria are the same as we used in our previous studies [4,11]:

1. Latitude:  $\pm 25^\circ$ ;
2. TB11 (M15, center wavelength  $10.7 \mu\text{m}$ )  $\leq 205 \text{ K}$ ;
3.  $\sigma$  (TB11) of the subject pixel and its eight adjacent pixels  $\leq 1 \text{ K}$ ;
4.  $\sigma$  (ref) of the subject pixel and its eight adjacent pixels  $\leq 3\%$ ;
5. Solar zenith angle (SZA)  $\leq 40^\circ$ ;
6. View zenith angle (VZA)  $\leq 35^\circ$ .

The anisotropic effects in the VIIRS VIS/NIR bands were corrected using an Angular Distribution Model (ADM) developed by Hu et al. [7]. A DCC seasonal cycle climatology derived using 4 years of NOAA version 2 reprocessed S-NPP VIIRS SDRs was used to further reduce the seasonal cycles in the daily and monthly DCC time series for both NOAA-20 and S-NPP VIIRS [4]. The mean and mode of the band-averaged daily and monthly DCC statistics (mean and mode) were calculated and used for characterizing VIIRS RSB long-term calibration stability, biases between different VIIRS SDRs, and inter-channel calibration consistency of the VIIRS RSBs. The mode of daily/monthly DCC reflectance was used for the VIS/NIR individual-band calibration stability assessment, while the mean of the daily/monthly DCC reflectance was used for the assessment of SWIR individual bands. Moreover, detector-level monthly DCC time series were used to assess detector-dependent degradation trends in the SDR products.

The mean of the DCC reflectance was also used to calculate the band ratio time series for inter-satellite or inter-SDR comparisons. The spectral differences between NOAA-20 and S-NPP VIIRS spectral bands (see Table 1) were corrected using the Spectral Band Adjustment Factors (SBAF), which are computed from algorithms and online tools developed at NASA-LaRC with the SCanning Imaging Absorption SpectroMeter for Atmospheric CHartographY (SCIAMACHY) V7.01 data obtained from the European Space Agency Envisat program [53,54].

Besides assessing the long-term calibration stability and biases, we also evaluated the VIIRS RSB inter-channel consistency using multi-year SCIAMACHY spectra-derived pseudo-reflectance, which were calculated with SCIAMACHY DCC spectra and NOAA-20/S-NPP VIIRS RSRs using the NASA SCIAMACHY spectra tool [53,54]. Only SCIAMACHY spectra within the range of VIIRS DCC observation-derived solar zenith angle, solar azimuth angle, and sensor view zenith angle were used. For VIIRS VIS/NIR bands, the averaged DCC reflectance was calculated using the monthly DCC mode time series. For VIIRS SWIR bands, the averaged DCC reflectance was calculated using the monthly DCC mean time series.

There is a concern about the impacts of VIIRS RSB saturations on the results of DCC trending. In this study, we analyzed DCC radiances for S-NPP and NOAA-20 during 2012 and 2021 using the reference band-based method developed in [55]. Our results indicate that there is no significant RSB saturation over DCCs for the VIIRS dual-grain bands (M1–M5 and M7). For the single-gain RSBs, only M6 has a low saturation radiance [55], and it is not considered in this study. More analysis results about VIIRS radiances over DCCs will be given in Section 4.5.

## 4. Results and Discussions

### 4.1. S-NPP VIIRS RSB SDRs

#### 4.1.1. Long-Term Calibration Stabilities of S-NPP VIIRS RSB SDRs

Ten years of S-NPP VIIRS observations are available to date. The long-term calibration stability of S-NPP VIIRS SDRs was evaluated using a monthly DCC time series. Figure 1 shows the VIS/NIR band monthly DCC time series for (a) NOAA-NPP-V2 (2/2012–12/2021, 9 years), (b) NASA-NPP-C1 (2/2012–12/2021, 10 years), and (c) NASA-NPP-C2 (2/2012–12/2021, 10 years). The trends and 95% confidence intervals (CI) for the three datasets and two time periods (2012–2020 and 2012–2021) are summarized in Table 3. The trends for the NOAA-NPP-OPR M-band RSB SDRs are also given in this table for comparison purposes only. The long-term DCC time series for the operational NOAA-NPP-OPR trending at NOAA STAR was generated using a similar DCC method as the monthly DCC method used in this study, except that only a quarter

of the global DCC pixels (latitude: 25°S to 25°N; longitude: 150°W to 60°W) were used [11], due to computing resource limitations. Our analysis results indicated that the trends derived were generally consistent with those derived using global DCCs, while the uncertainty of the trends was larger [5] because of the smaller number of DCC pixels used. In addition, long-term DCC time series for NOAA-NPP-OPR I-band RSBs (I1–I3) were not available.

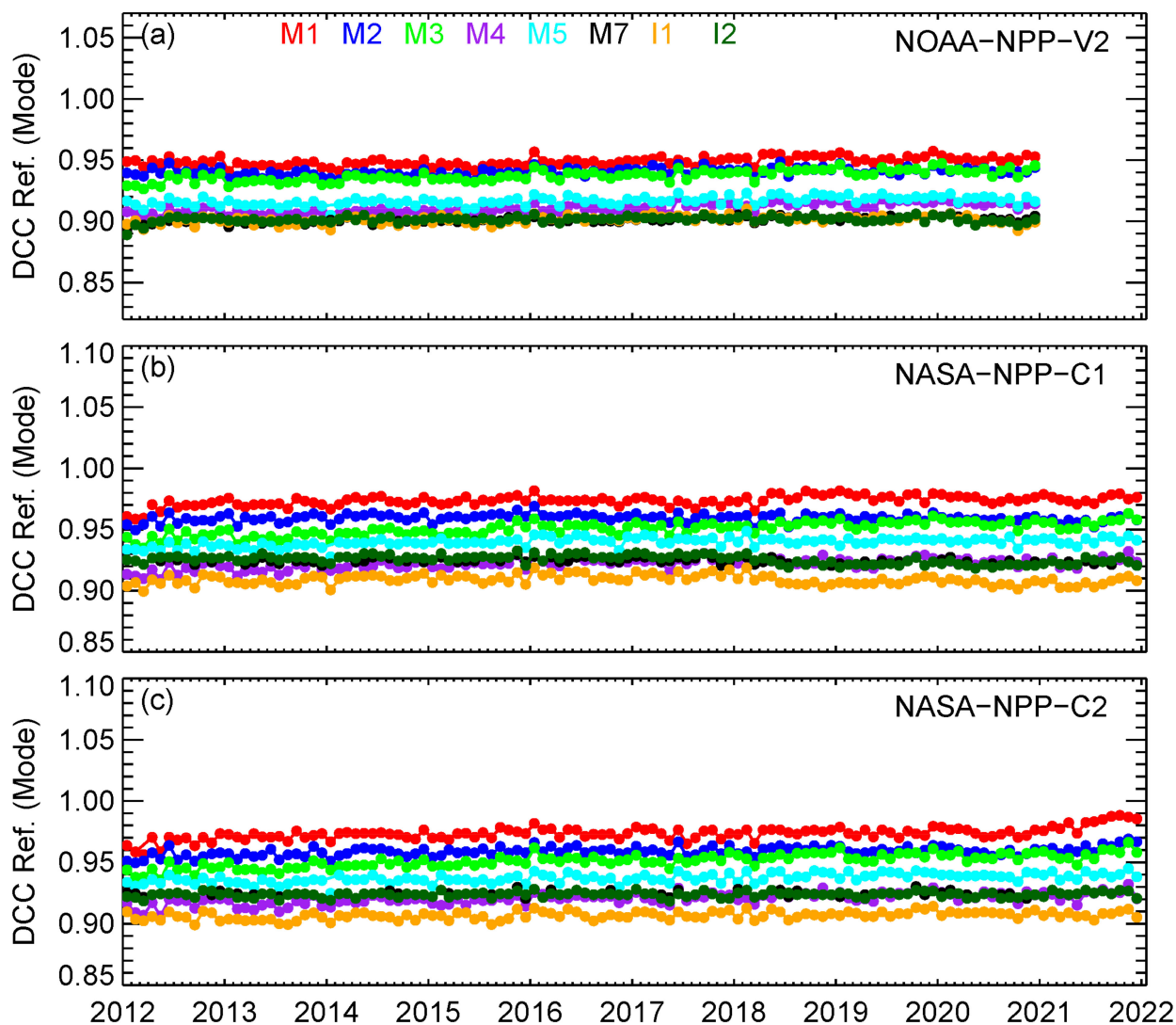


**Figure 1.** Monthly DCC time series of S-NPP VIIRS VIS/NIR bands: (a) NOAA-NPP-V2 (2012–2020), (b) NASA-NPP-C1 (2012–2021), and (c) NASA-NPP-C2 (2012–2021).

Our results suggest that the three reprocessed S-NPP VIS/NIR band SDRs evaluated in this study are generally stable in NOAA and NASA processing, with trends within 0.1%/year for the majority of the bands. No significant trend was observed in three NOAA-NPP-V2 bands (I2, M9, and M11); five NASA-NPP-C1 bands (M2, I1, and M9–M11); and seven NASA-NPP-C2 bands (M7, I2, M8–M11, and I3). The trends in the remaining bands are significant (exceeding the 95% CIs). The 10 years of NOAA-NPP-OPR M5 and M7 SDRs are also stable, with no obvious trends observed. The trends for NOAA-NPP-OPR M3 ( $\sim -0.1\%/year$ ) are smaller than those in NOAA-NPP-V2/NASA-NPP-C1/NASA-NPP-C2. The trends for M1 and M4 are comparable to the three reprocessed data records. On the other hand, larger trends were observed in NOAA-NPP-OPR M2 and M8–M9, with trends up to  $\sim 0.2\%/year$  for M2.

**Table 3.** Summary of the trends and 95% confidence intervals (CI) of S-NPP VIIRS RSB SDRs generated by NOAA and NASA. Cases with trends larger than 0.1%/year are in bold.

| Trend $\pm$ 95% CI<br>Unit: %/year | NOAA-NPP-OPR<br>2012–2020/2012–2021                 | NOAA-NPP-V2<br>2012–2020 | NASA-NPP-C1<br>2012–2020/2012–2021                  | NASA-NPP-C2<br>2012–2020/2012–2021                |
|------------------------------------|---|--------------------------|---|---|
| M1                                 | $-0.07 \pm 0.05 / -0.04 \pm 0.04$                   | $0.08 \pm 0.02$          | $0.07 \pm 0.02 / 0.06 \pm 0.02$                     | $0.05 \pm 0.03 / \mathbf{0.11 \pm 0.03}$          |
| M2                                 | $-\mathbf{0.20 \pm 0.04} / -\mathbf{0.18 \pm 0.04}$ | $0.05 \pm 0.02$          | $0.01 \pm 0.02 / -0.01 \pm 0.02$                    | $0.05 \pm 0.02 / 0.06 \pm 0.02$                   |
| M3                                 | $-\mathbf{0.11 \pm 0.04} / -0.09 \pm 0.04$          | $\mathbf{0.14 \pm 0.02}$ | $\mathbf{0.17 \pm 0.03} / \mathbf{0.15 \pm 0.02}$   | $\mathbf{0.16 \pm 0.02} / \mathbf{0.16 \pm 0.02}$ |
| M4                                 | $-\mathbf{0.14 \pm 0.04} / -\mathbf{0.11 \pm 0.04}$ | $\mathbf{0.13 \pm 0.02}$ | $\mathbf{0.11 \pm 0.03} / 0.09 \pm 0.02$            | $\mathbf{0.13 \pm 0.03} / \mathbf{0.11 \pm 0.02}$ |
| M5                                 | $0.00 \pm 0.03 / 0.01 \pm 0.03$                     | $0.07 \pm 0.02$          | $0.07 \pm 0.02 / 0.06 \pm 0.02$                     | $0.08 \pm 0.02 / 0.08 \pm 0.02$                   |
| M7                                 | $0.00 \pm 0.03 / 0.00 \pm 0.03$                     | $0.05 \pm 0.01$          | $-0.03 \pm 0.02 / -0.03 \pm 0.02$                   | $0.01 \pm 0.02 / 0.01 \pm 0.01$                   |
| I1                                 | -   | $0.05 \pm 0.02$          | $-0.01 \pm 0.03 / -0.02 \pm 0.03$                   | $0.06 \pm 0.02 / 0.05 \pm 0.02$                   |
| I2                                 | -   | $0.01 \pm 0.02$          | $-0.07 \pm 0.02 / -0.06 \pm 0.02$                   | $0.01 \pm 0.02 / 0.01 \pm 0.01$                   |
| M8                                 | $\mathbf{0.12 \pm 0.07} / \mathbf{0.14 \pm 0.06}$   | $-0.05 \pm 0.04$         | $-0.07 \pm 0.04 / -0.05 \pm 0.03$                   | $-0.05 \pm 0.04 / -0.02 \pm 0.03$                 |
| M9                                 | $\mathbf{0.18 \pm 0.14} / \mathbf{0.19 \pm 0.12}$   | $-0.03 \pm 0.06$         | $0.01 \pm 0.07 / 0.04 \pm 0.06$                     | $-0.02 \pm 0.07 / 0.01 \pm 0.06$                  |
| M10                                | $\mathbf{0.12 \pm 0.15} / \mathbf{0.13 \pm 0.12}$   | $-0.09 \pm 0.05$         | $-0.06 \pm 0.06 / -0.02 \pm 0.05$                   | $-0.06 \pm 0.06 / 0.00 \pm 0.05$                  |
| M11                                | $0.09 \pm 0.13 / 0.09 \pm 0.10$                     | $-0.05 \pm 0.05$         | $-0.04 \pm 0.05 / -0.02 \pm 0.04$                   | $-0.04 \pm 0.05 / -0.01 \pm 0.04$                 |
| I3                                 | -   | $-0.09 \pm 0.06$         | $-\mathbf{0.19 \pm 0.07} / -\mathbf{0.15 \pm 0.04}$ | $-0.05 \pm 0.06 / -0.02 \pm 0.05$                 |

The DCC trending results derived in this study are generally consistent with an existing study [56], which reported that the 10-year NASA-NPP-C2 RSB VIS/NIR SDRs are stable within 1% based on PICS-based approaches. However, our DCC time series showed that M3–M4 trends exhibited persistent larger trends in all three data records evaluated, ranging from 0.11 to 0.17%/year. In addition, M3 showed larger trends than M4. Figure 2 shows a normalized monthly DCC time series for the two bands to better reveal the trends. The mode of monthly DCC reflectance was normalized to the first data point (February 2012). Lunar-based F-factors are also used for the long-term calibrations of M3–M4 [5,23,26]. VIIRS lunar observations were at a high gain (HG, low radiance) while the DCC observations were at a low gain (LG, high radiance) for the dual-gain VIS/NIR bands, such as M3 and M4. We compared the prelaunch test data-derived nonlinearity of the S-NPP VIS/NIR bands. The results indicate that the HG and LG nonlinearities for M3–M4 (especially M3) have significantly larger differences compared to the other VIS/NIR bands. The rates of instrument responsivity degradation in LG and HG may also be different. The results from this study indicate that the Lunar-based F-factors may not work well for the S-NPP M3–M4 at LG. We will further discuss this topic in Section 4.2.1.

Moreover, relatively larger separations between the NOAA-NPP-V2 and NASA-NPP-C1/C2 M4 normalized DCC time series were observed from mid-2013 to early 2017. The root cause of the separations is still unknown. Our previous study indicated that NASA-NPP-C1/C2 F-factors in the beginning of the mission show larger curvature, while NOAA-NPP-V2 F-factors are more flat [5]. The F-factor difference may cause a separation of the DCC time series after they are normalized to the first point. Moreover, NOAA-NPP-V2 DCC time series were generally stable during 2013–2015, while the NASA-NPP-C1/C2 DCC time series showed gradual trends during the same period. We will further investigate the root cause in the future.

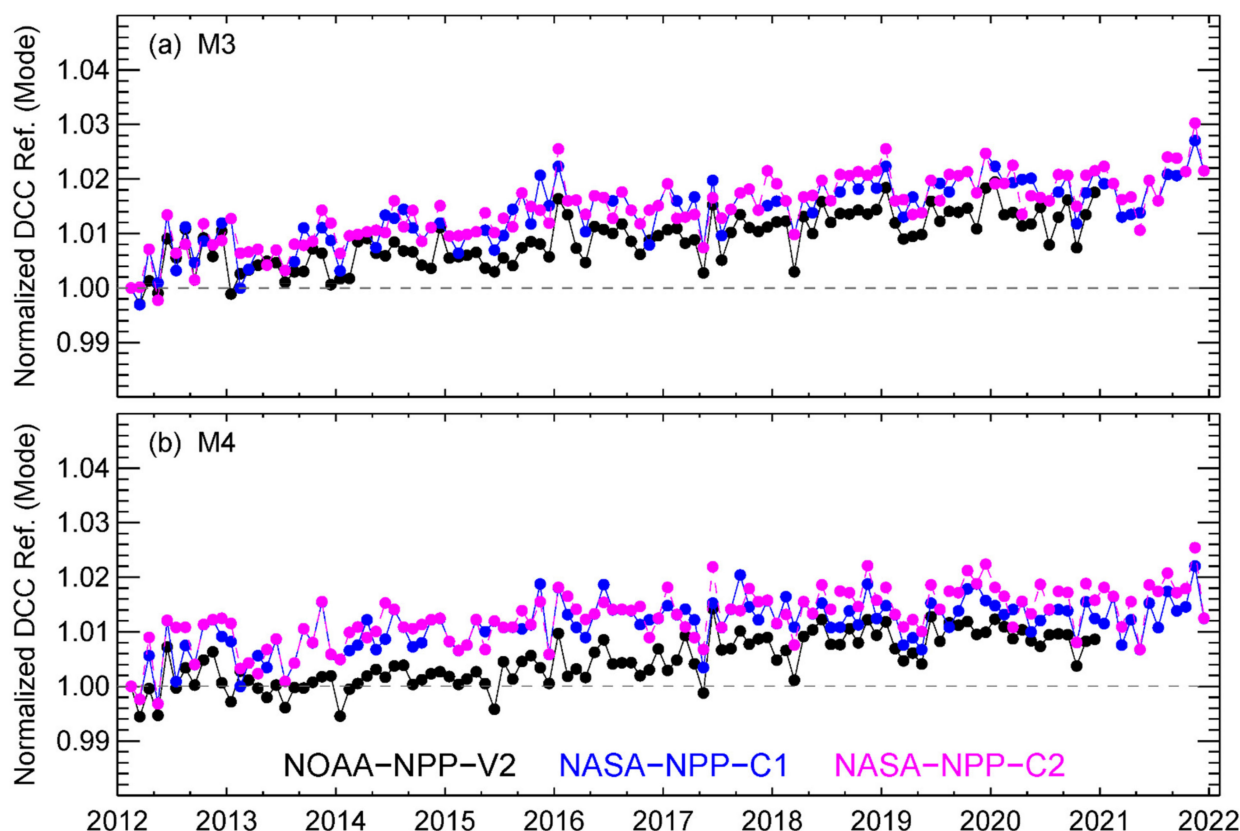


**Figure 2.** Normalized monthly DCC time series for S-NPP VIIRS bands (a) M3 and (b) M4. All data points are normalized to February 2012.

Besides M3–M4, the NASA-NPP-C2 2012–2021 M1 DCC time series also showed a relatively larger trend (0.11%/year) compared to the trends in the 2012–2020 time series and in the NASA-NPP-C1 data. The larger NASA-NPP-C2 M1 trend was mainly caused by the 2021 data (see Figure 1c), with the DCC reflectance obviously higher than the previous 9 years. In addition, the monthly DCC reflectance of the first two months (February and March 2012) in the NASA-NPP-C1/NASA-NPP-C2 M1–M3 and NOAA-NPP-V2 M3 and I2 time series were  $\sim 1\%$  lower than that of the other months and may require further study.

The long-term calibration trends of the S-NPP VIIRS SWIR SDRs were also very stable, with trends less than 0.1%/year in all the bands, except I3 of NASA-NPP-C1 (see Table 3). The M8–M11 stability of the NASA-NPP-C1 and NASA-NPP-C2 SWIRs were very close to each other. The calibration stability of I3 was significantly improved in the NASA-NPP-C2 data, with the trend reduced from  $\sim 0.15\%/year$  to  $-0.02\%/year$  for the 10-year data records. Our analysis results showed that the DCC reflectances for the two SDRs were very close to each other from early 2018 to 2021. There were larger differences from 2012 to 2017, with the NASA-NPP-C1 I3 DCC reflectances higher than NASA-NPP-C2. Bands M10 and I3 of the NOAA-NPP-V2 also showed relatively larger trends ( $-0.09 \pm 0.06\%/year$ ). The 95% CIs indicate that the trends in the two bands are significant.

#### 4.1.2. Detector Level Calibration Stability of S-NPP VIIRS SDRs

In Section 4.1.1, the band-averaged (averaged over all detectors) monthly DCC time series showed that the calibrations of three S-NPP VIIRS RSB SDRs are generally stable. This subsection looks into the S-NPP VIIRS RSB residual degradations at the individual detector levels. Figure 3 shows an example of the M1 detector level monthly DCC time series for the three SDRs. It can be observed that the detector level DCC reflectance values are more consistent with each other near the beginning of the mission, with the divergence within

1%. However, the detector-level divergence increased over time, especially in NOAA-NPP-V2 (Figure 3a) and NASA-NPP-C1 (Figure 3b). Similar patterns were observed in bands M2–M4, though the magnitudes of divergence were smaller in M3–M4. The results for NASA-NPP-C1 are generally consistent with the detector-to-detector differences reported by [13,16,43]. On the other hand, the detector level divergence is much smaller in the NASA-NPP-C2 dataset (see Figure 3c), due to the removal of striping caused by nonuniform degradation of the SD [13,23,42,43]. Upward trends in the NASA-NPP-C2 M1 DCC detector level reflectance was observed since early 2021, which are mainly caused by the increase of F-factors used in the calibrations. No similar increase of F-factors was observed in the other NASA-NPP-C2 RSBs. The detector-level calibrations of other RSBs (M5, M7, and I1–I2) and all SWIR bands are more consistent in the three S-NPP SDRs. In addition, the magnitude of detector-level divergences in NOAA-NPP-OPR RSB SDRs are similar to those in NOAA-NPP-V2.

For the NOAA-NPP-V2 M1–M4, the calibrations of the middle detectors (D6–D9) are generally more stable than that of the edge detectors (such as D1–D2 and D15–D16), which show detector level degradations up to  $\sim\pm 1.5\%$  for M1–M2 and  $\sim\pm 1\%$  for M3–M4, relative to the middle detectors. Similar larger degradations for the edge detectors were also observed in NASA-NPP-C1 M1–M4. While the detector-dependent degradations do not have a significant impact on downstream applications that mix data from all detectors, they do cause striping in the VIIRS RSB imagery and affect applications using individual pixels.

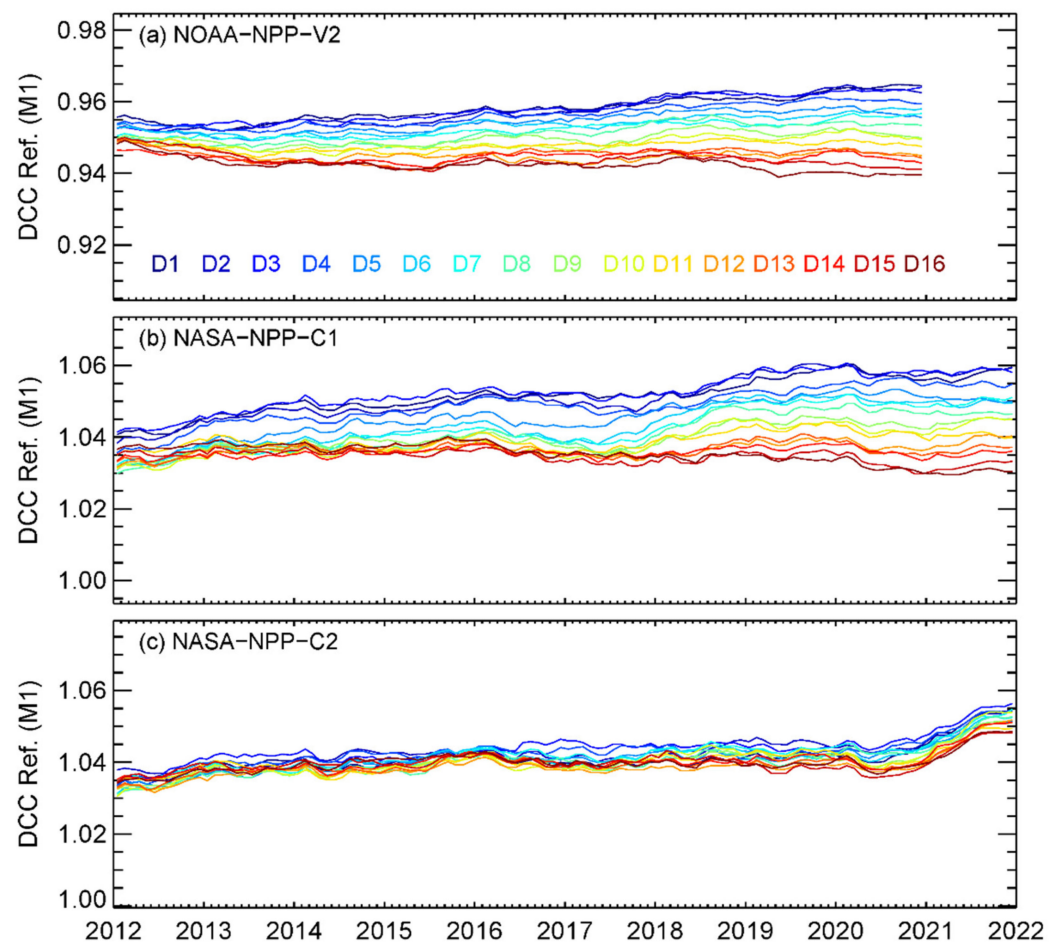
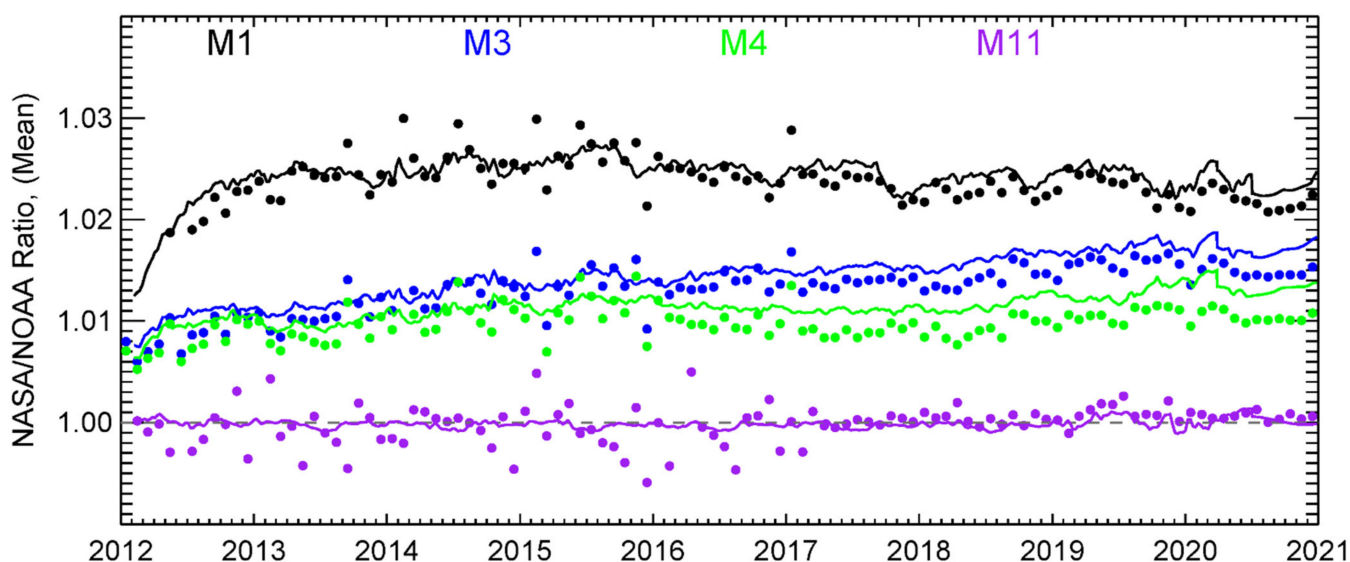


Figure 3. Detector level monthly DCC time series for S-NPP VIIRS M1.

#### 4.1.3. NASA/NOAA S-NPP VIIRS RSB Calibration Biases

While the long-term calibration stabilities of the three S-NPP VIIRS RSB SDRs are similar, calibration biases exist between the NOAA and NASA data. The 2012–2020 averaged biases between the NASA-NPP-C2 and NOAA-NPP-V2 RSB SDRs were about 2.3% (M1), 1.8% (M2), 1.5% (M3), 1.0% (M4), 2.3% (M5), 2.4% (M7), 0.2% (M8), 0.3% (M9), 0.7% (M10), 0.1% (M11), 0.3% (I1), 2.0% (I2), and 0.6% (I3). The VIS/NIR bands exhibited larger biases (up to 2.4%) compared to the SWIR bands (up to 0.7%). Moreover, the biases were nearly constant over time for the majority of bands.

Figure 4 compares the DCC and F-factor ratio time series between NASA-NPP-C2 and NOAA-NPP-V2 for the representative bands. It can be observed that the DCC ratio time series followed closely by the F-factor ratio time series, indicating that the biases between two SDR products are primarily caused by the F-factors developed by NOAA and NASA science teams. M1 and M11 DCC and the F-factor ratio time series are more consistent with each other, while the M3–M4 F-factor ratios are slightly higher than DCC ratios. The biases between NASA-NPP-C2 and NASA-NPP-C1 SWIR RSB SDRs are very small.



**Figure 4.** NASA-NPP-C2/NOAA-NPP-V2 ratio time series for bands M1, M3–M4, and M11: filled cycles (DCC ratio) and solid lines (F-factor ratio).

#### 4.2. NOAA-20 VIIRS RSB SDRs

##### 4.2.1. Long-Term Calibration Stabilities of NOAA-20 VIIRS SDRs

Different from S-NPP VIIRS, the on-orbit degradation of NOAA-20 VIIRS VIS/NIR bands has been very small since the launch [3,4,44,52]. Figure 5 shows the monthly VIS/NIR DCC time series for the NOAA-N20-ConstF and NASA-N20-C2 VIIRS SDR products. The long-term calibration stabilities for all RSBs are summarized in Table 4. Since there are only 4 years of NOAA-20 data records available to date, we also analyzed the daily DCC time series for NOAA-20. The trends derived using the daily and monthly DCC methods are very close. The uncertainties of trends derived using daily DCC time series are smaller than those derived using a monthly DCC time series, consistent with the results reported in our previous study [4]. In addition, 2018–2021 trends for the NOAA-N20-OPR were also evaluated using the same daily and monthly DCC methods used for NOAA-N20-ConstF and NASA-N20-C2, and the results are also given in Table 4. Note that significant calibration changes exist in the operational processing before NOAA-20 VIIRS achieved validated maturity status (30 April 2018) [4]. The NOAA-N20-OPR trends are for comparison purposes only.

Small downward trends exist in the NOAA-20 VIS/NIR DCC time series in both NOAA-N20-ConstF and NASA-N20-C2 SDRs. However, the trends for the NOAA-N20-ConstF SDRs are insignificant for all bands, except I1. The trends in I1 are significant (exceeding the 95% CIs):  $-0.08 \pm 0.04\%/year$  (daily DCC time series) and  $0.10 \pm 0.08\%/year$  (monthly DCC time series). The trends in the NOAA-N20-ConstF VIS/NIR DCC time series are generally consistent with the lunar calibration results from the NOAA VIIRS SDR science team. Note that constant F-factors were used in NOAA operational processing from 27 April 2018 to 4 November 2021. Based on the lunar and DCC trending results, small upward trends were introduced to the NOAA operational VIS/NIR F-factors since 4 November 2021 to correct the small trends in the VIS/NIR bands, but the impact of the update on this study can be ignored. Note that the DCC and lunar trending results do not agree in S-NPP VIIRS bands M3–M4. However, no such disagreement was found in the NOAA-N20-ConstF M3–M4 SDRs.

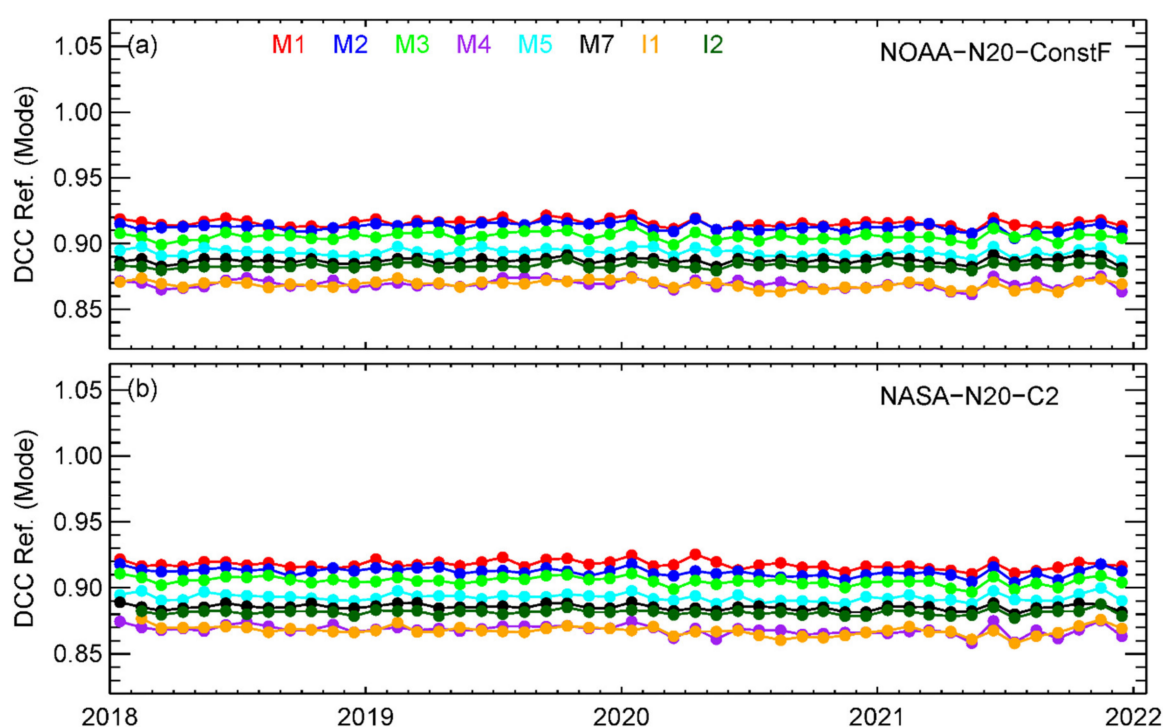


**Figure 5.** NOAA-20 VIIRS VIS/NIR bands monthly DCC time series: (a) NOAA-N20-ConstF and (b) NASA-N20-C2.

Relatively larger downward trends exist in the NASA-N20-C2 VIS/NIR DCC time series, especially for bands M2–M4 and I1. The trends in the I1 daily ( $-0.1\%/year$ ) and monthly ( $-0.17\%/year$ ) DCC times are significant and similar to those of NOAA-N20-ConstF. The trends in M2–M4 ( $-0.1$ – $-0.15\%/year$ ) are also significant, with trends exceeding the 95% CIs for both the daily and monthly DCC time series. Twedt et al. [46] evaluated the NASA-N20-C2 RSB trends over the Libyan-4 desert site and DCCs for the first three years of the mission. Similar small downward trends in VIS/NIR SDRs were reported (less than  $0.2\%/year$ ).

The trends in NOAA-N20-OPR VIS/NIR SDRs are much larger than those in NOAA-N20-ConstF and NOAA-N20-C2 for the majority of bands. Only M5 and M7 are stable and comparable to the two reprocessed SDRs. M1–M4 and I1–I2 exhibit significant trends (up to  $\sim 0.3\%/year$  in M1) because of the operational calibration updates during the early NOAA-20 mission. Note that the calibration of NOAA-N20-OPR RSB SDRs from May to December, 2021 are stable and consistent with the NOAA-N20-ConstF data.

Different from the small downward trends in the NOAA-20 VIIRS VIS/NIR bands, small upward trends were observed in the NOAA-N20-ConstF and NASA-N20-C2 SWIR

SDRs. However, these trends are within or only slightly above the uncertainty levels. M10 and I3 show relatively larger trends in both NOAA and NASA SDRs. NASA-N20-C2 M8 and M11 also exhibit trends slightly higher than the uncertainty levels in the daily DCC time series. The NASA-N20-C2 M8 trends are similar to the values reported by [46]. For M10/I3, the trends derived in this study are larger ( $\sim 0.15\%/year$ ), while no significant was reported by [46]. On the contrary, significant trends were observed in the NOAA-N20-OPR M9–M11 and I4 SDRs, more than  $0.3\%/year$  in M10 and I3. These larger trends are also caused by the operational calibration updates in the early NOAA-20 mission. Similar to the VIS/NIR bands, the SWIR trends derived using daily and monthly DCC time series are generally consistent with each other.

**Table 4.** Summary of the trends and 95% confident intervals (CI) of NOAA-20 VIIRS RSB DCC time series for the NOAA-N20-ConstF and NASA-N20-C2 products. Cases with trends beyond the uncertainty levels are in bold.

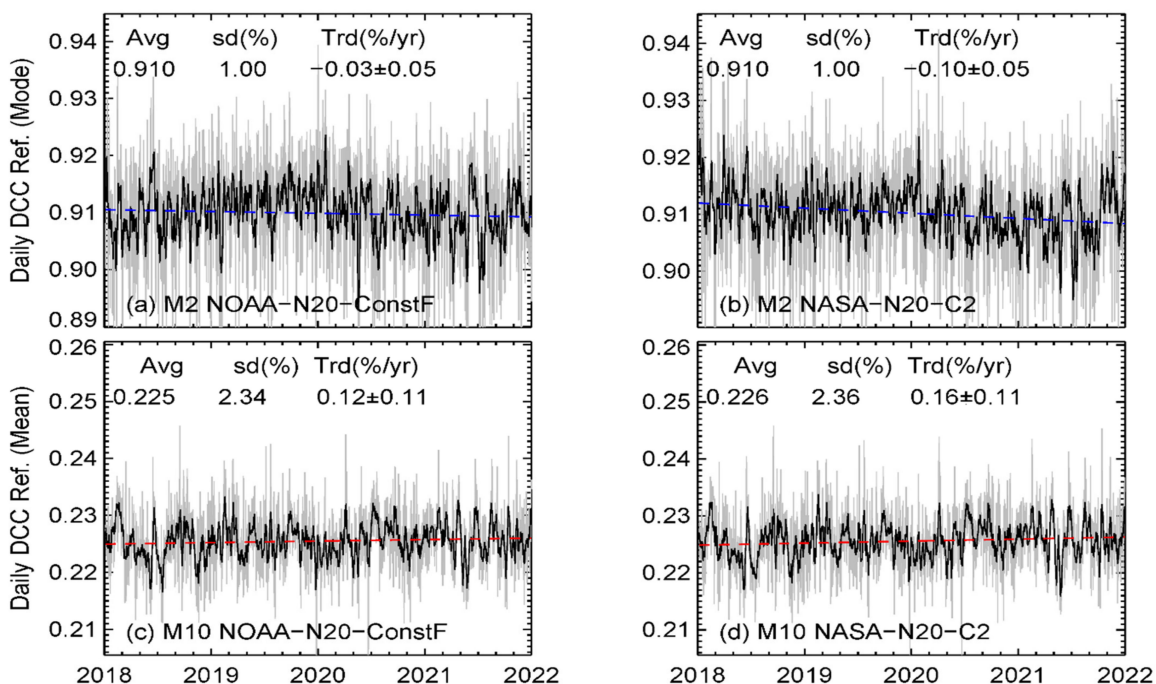
|      | Trend $\pm$ 95%CI Unit:<br>%/year | NOAA-N20-OPR<br>Daily/Monthly     | NOAA-N20-ConstF<br>Daily/Monthly  | NASA-N20-C2<br>Daily/Monthly      |
|------|-----------------------------------|-----------------------------------|-----------------------------------|-----------------------------------|
| VNIR | M1                                | $-0.29 \pm 0.05 / -0.16 \pm 0.14$ | $-0.00 \pm 0.04 / -0.05 \pm 0.08$ | $-0.05 \pm 0.05 / -0.10 \pm 0.08$ |
|      | M2                                | $-0.20 \pm 0.05 / -0.11 \pm 0.10$ | $-0.03 \pm 0.05 / -0.08 \pm 0.08$ | $-0.10 \pm 0.05 / -0.13 \pm 0.08$ |
|      | M3                                | $-0.17 \pm 0.05 / -0.17 \pm 0.11$ | $-0.01 \pm 0.05 / -0.02 \pm 0.09$ | $-0.12 \pm 0.05 / -0.12 \pm 0.08$ |
|      | M4                                | $-0.14 \pm 0.05 / -0.16 \pm 0.11$ | $-0.03 \pm 0.05 / -0.05 \pm 0.10$ | $-0.13 \pm 0.05 / -0.15 \pm 0.10$ |
|      | M5                                | $-0.05 \pm 0.04 / -0.06 \pm 0.09$ | $-0.04 \pm 0.04 / -0.07 \pm 0.08$ | $-0.07 \pm 0.04 / -0.06 \pm 0.08$ |
|      | M7                                | $0.03 \pm 0.03 / 0.05 \pm 0.07$   | $0.01 \pm 0.03 / 0.03 \pm 0.07$   | $-0.05 \pm 0.03 / -0.06 \pm 0.06$ |
|      | I1                                | $-0.08 \pm 0.04 / -0.11 \pm 0.08$ | $-0.08 \pm 0.04 / 0.10 \pm 0.08$  | $-0.10 \pm 0.05 / -0.17 \pm 0.09$ |
|      | I2                                | $-0.08 \pm 0.03 / -0.13 \pm 0.09$ | $-0.01 \pm 0.03 / 0.01 \pm 0.06$  | $-0.02 \pm 0.03 / -0.04 \pm 0.05$ |
| SWIR | M8                                | $-0.03 \pm 0.05 / -0.04 \pm 0.15$ | $0.01 \pm 0.05 / 0.00 \pm 0.15$   | $0.06 \pm 0.05 / 0.04 \pm 0.15$   |
|      | M9                                | $0.18 \pm 0.11 / 0.10 \pm 0.24$   | $0.05 \pm 0.10 / 0.05 \pm 0.23$   | $0.09 \pm 0.10 / 0.08 \pm 0.23$   |
|      | M10                               | $0.31 \pm 0.11 / 0.15 \pm 0.23$   | $0.12 \pm 0.11 / 0.09 \pm 0.24$   | $0.16 \pm 0.11 / 0.14 \pm 0.24$   |
|      | M11                               | $0.18 \pm 0.09 / 0.05 \pm 0.20$   | $0.04 \pm 0.08 / 0.01 \pm 0.24$   | $0.14 \pm 0.09 / 0.12 \pm 0.20$   |
|      | I3                                | $0.36 \pm 0.11 / 0.22 \pm 0.23$   | $0.14 \pm 0.11 / 0.11 \pm 0.24$   | $0.16 \pm 0.11 / 0.13 \pm 0.25$   |

Figure 6 shows examples of the daily DCC time series for bands M2 and M10. Raw daily DCC time series are shown by gray lines. Black lines are moving averages with a window size of 7 days to better reveal the time-dependent trends in the daily DCC time series. Overall, there is no significant trend in the NOAA-N20-ConstF M2 daily DCC time series, while NASA-N20-C2 M2 shows a relatively larger downward trend of  $-0.10\%/year$ , exceeding the uncertainty level. The NOAA M2 daily DCC time series also revealed that the trends vary with time, with a smaller upward trend during 2018–2019, a small downward trend in 2020, and mostly flat response in 2021. M10 SDRs generated by NOAA and NASA are close to each other, with a small upward in the daily DCC time series ( $0.12\%/year$  for NOAA-N20-ConstF and  $0.16\%/year$  for NASA-N20-C2).

Note that significant detector-level residual degradations were observed in S-NPP M1–M4. We also analyzed the NOAA-20 VIIRS detector-level monthly DCC time series. The results indicate that no significant detector level degradation was found in NOAA-20 RSB SDRs, different from S-NPP. SDR imagery analysis further confirms that no obvious striping exists in NOAA-20 VIIRS RSBs.

#### 4.2.2. NASA/NOAA NOAA-20 VIIRS Calibration Biases

We also analyzed the calibration consistency between NOAA and NASA NOAA-20 VIIRS RSB SDRs over DCCs. Figure 7 shows the NASA/NOAA DCC ratio time series. Different from S-NPP VIIRS, NOAA-20 VIIRS RSB SDRs generated by the two agencies show very good agreement, with averaged biases within 0.2% for M-band RSBs and within 0.7% for I-band RSBs. The M-band biases derived in this study are consistent with a previous study, while I1–I3 biases over DCCs are slightly larger [57]. In addition, the biases are nearly constant over time for the majority of the bands. The biases in I1–I2 decrease significantly during September–November 2021 compared to the previous months. We also compared the NASA/NOAA F-factors ratio time series to the daily DCC ratio time series. The two ratio time series match well with each other.



**Figure 6.** Examples of daily DCC time series for NOAA-20 VIIRS M2 and M10. Raw daily DCC time series are shown by gray lines. Black lines are moving averages with a window size of 7 days. Linear regression trends are shown as blue (downward trend) or red (upward trend) dashed lines.

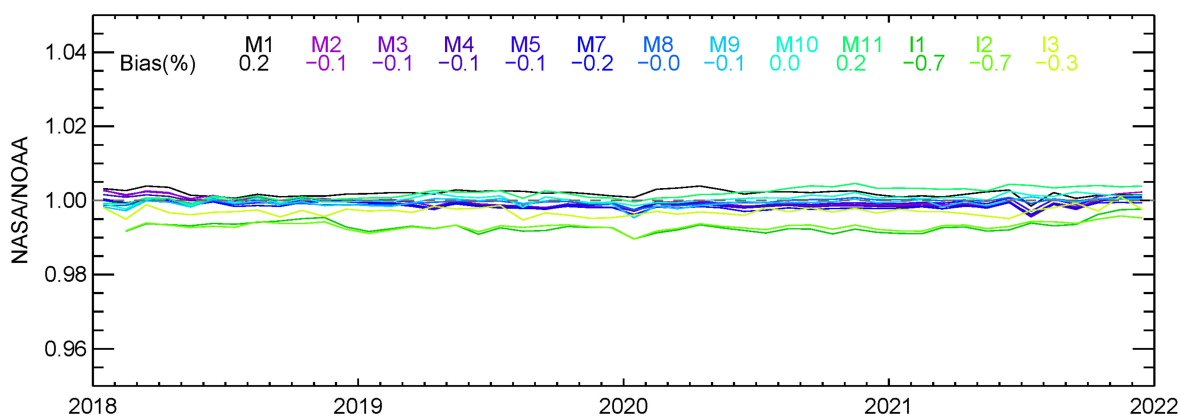


**Figure 7.** Monthly DCC ratio time series for the NASA-N20-C2 and NOAA-N20-ConstF SDRs.

#### 4.3. Inter-Satellite Biases between NOAA-20 and S-NPP VIIRS RSBs

While the NOAA and NASA-generated VIIRS RSB SDRs are generally stable, their absolute radiometric calibration accuracies are still not well-quantified to date. NOAA-20 and S-NPP VIIRS inter-satellite biases show how the measurements from two VIIRS sensors agree with each other and, therefore, may provide some useful information about their absolute calibration accuracy. Figure 8 shows inter-satellite biases between the S-NPP and NOAA-20 VIIRS RSBs in the NOAA and NASA SDRs for M-band RSBs. Intersatellite biases for all RSBs are given in Table 5. The biases between NOAA-NPP-OPR and NOAA-N20-OPR (May 2018–December 2021) are also listed in Table 5 for comparison purposes only. The S-NPP RSB reflectances are higher than that of NOAA-20 over the DCCs for all NOAA and NASA-produced SDRs.

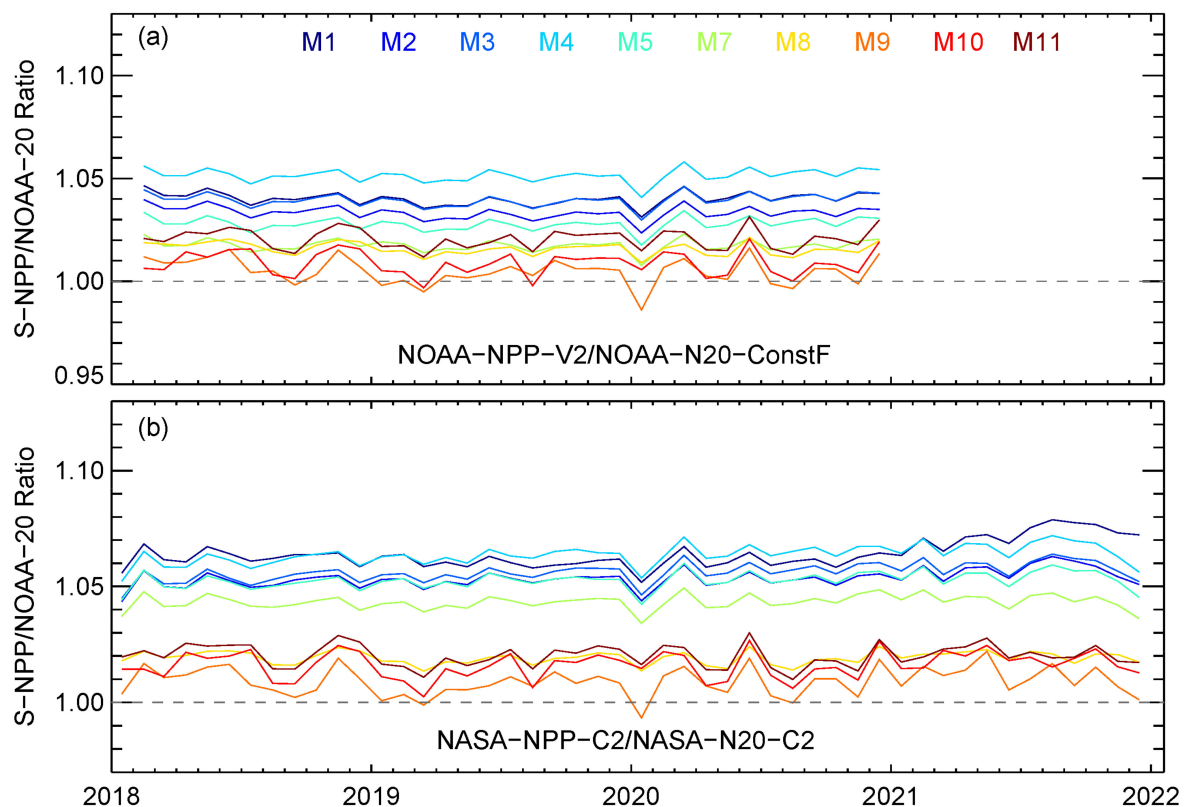


**Figure 8.** NOAA-20 and S-NPP VIIRS inter-satellite biases: (a) NOAA-NPP-V2/NOAA-N20-ConstF and (b) NASA-NPP-C1/NASA-N20-C2.

The biases between NOAA-NPP-V2 and NOAA-N20-ConstF are up to 4.5%. Moreover, the biases were nearly constant from 2018 to 2020. Bands M1, M4, and I1 exhibited larger biases, more than 4%. The biases in the NOAA operational SDRs were also nearly constant from May 2018 to December 2021, consistent with the results from previous studies. The DCC-based biases in the operational data presented here are consistent with those reported in our previous study [52]. While the NOAA-N20-ConstF RSB SDRs are very close to the NOAA-N20-OPR data after 30 April 2018, the NOAA-NPP-V2 SDRs are significantly different from the operational version. For M1–M4 and I1, the biases between NOAA-NPP-V2 and NOAA-N20-ConstF are higher than those in the operational data. For M5, M7–M11, and I2–I3, the biases are ~1.5–2% lower than the biases in the operational data [5]. RSB biases in the NOAA operational SDRs were also analyzed over SNO/SNO-x (with Aqua MODIS/GOES-R ABI as the transfer radiometers) [58,59], the Libyan-4 site [52,58], and the Dome-C site [52]. For the NOAA operational SDRs, the biases derived using the DCC method are generally consistent with those derived other methods, with differences within  $\pm 1\%$  in the majority of cases. The NOAA-20 and S-NPP inter-satellite biases are likely caused by the differences in the

prelaunch calibration methodologies used for characterizing the SD Bidirectional Reflectance Factor (BRF) [60].

**Table 5.** Summary of the NOAA-20 and S-NPP inter-satellite biases in the NOAA and NASA-generated VIIRS RSB SDRs.

| Biases (%) | NOAA-NPP-OPR/<br>NOAA-N20-OPR<br>(5/2018–2021) | NOAA-NPP-V2/<br>NOAA-N20-ConstF<br>(2018–2020) | NASA-NPP-C1/<br>NASA-N20-C2 (2018–2021) | NASA-NPP-C2/<br>NASA-N20-C2 (2018–2021) |
|------------|--|--|---|---|
| M1         | 3.6  | 4.3  | 7.0                                     | 6.7                                     |
| M2         | 1.9  | 3.4  | 5.5                                     | 5.5                                     |
| M3         | 2.6  | 3.9  | 5.6                                     | 5.7                                     |
| M4         | 2.8  | 4.5  | 5.8                                     | 5.8                                     |
| M5         | 4.6  | 2.9  | 5.5                                     | 5.4                                     |
| M7         | 3.6  | 1.5  | 4.0                                     | 4.2                                     |
| I1         | 3.2  | 4.1  | 5.1                                     | 5.2                                     |
| I2         | 4.0  | 1.8  | 4.5                                     | 4.7                                     |
| M8         | 3.0  | 1.6  | 1.9                                     | 1.9                                     |
| M9         | 1.7  | 0.5  | 1.0                                     | 1.0                                     |
| M10        | 3.6  | 2.2  | 2.9                                     | 3.0                                     |
| M11        | 2.6  | 2.1  | 2.0                                     | 2.0                                     |
| I3         | 4.9  | 3.5  | 4.5                                     | 4.5                                     |

The inter-satellite biases in the NASA VIIRS RSB SDRs are even larger. The biases between NASA-NPP-C2 (or NASA-NPP-C1) and NASA-N20-C2 SDRs are higher than 4% in all VIS/NIRs and band I3. M1 exhibits the largest biases, 7% and 6.7%, for NASA-NPP-C1 and NASA-NPP-C2, respectively. The differences in the biases between NASA-NPP-C1/NASA-N20-C2 and NASA-NPP-C2/NASA-N20-C2 were very small (within 0.3%). Xiong et al. [56] analyzed M1–M2, M4, M7, and I1–I2 biases in the NASA NOAA-20 and S-NPP VIIRS SDRs, using observations over SNOs (with Aqua MODIS as the transfer radiometer), Libyan-4, and Dome-C. The M1–M2 and M7 biases over the DCCs derived in this study agree well with [56]. The M4 bias over DCCs is similar to that of the Dome-C site; both were ~2% higher than the biases over SNOs and Libyan-4. For I1–I2, the biases over DCCs were ~1% and 1.5% higher than the values reported by [56].

#### 4.4. Inter-Channel Calibration Consistency of NOAA-20 and S-NPP VIIRS RSBs

We also studied the inter-channel calibration consistency of the VIIRS RSB SDRs using SCIAMACHY spectra-derived DCC reflectance (convolved over VIIRS RSRs) as a reference. Figure 9 compares the VIIRS DCC reflectance with SCIAMACHY DCC reflectance for different NOAA-20 and S-NPP RSBs. The results for NASA-NPP-C1 are similar to that of NASA-NPP-C2; therefore, they are not shown. Note that NOAA-N20-ConstF and NASA-N20-C2 agree well with each other. For VIIRS VIS/NIR bands, the multiyear averaged DCC reflectance was estimated using monthly DCC mode time series. For VIIRS SWIR bands, the multiyear averaged DCC reflectance was estimated using a monthly DCC mean time series. M11 is not covered by the SCIAMACHY spectra; therefore, it was not considered.

The DCC reflectance of VIIRS RSBs correlates strongly with SCIAMACHY-derived DCC reflectance, with a correlation coefficient of ~0.995 for the three S-NPP VIIRS SDRs and ~0.993 for the two NOAA-20 VIIRS SDRs. The shape of NOAA-NPP-V2 DCC reflectance matches best with that of SCIAMACHY. The shape of the NASA-NPP-C2 DCC reflectance also matches well with SCIAMACHY, better than NOAA-20 SDRs. Thompson [61] analyzed the liquid and ice absorption of a cloud at a spectral range covered by VIIRS M10 and I3. The results showed that the TOA reflectance of icy cloud is ~0.2, very close to the VIIRS M10/I3 averaged DCC reflectance derived in this study and SCIAMACHY DCC reflectance.

The M4 and M9 reflectance over DCCs seems out of family in all five VIIRS SDRs evaluated. SCIAMACHY-observed DCC reflectance drops monotonically for spectral bands from 0.41  $\mu\text{m}$  (M1) to 0.86  $\mu\text{m}$  (M7). A similar monotonic drop of DCC reflectance for the similar spectral range was also reported by [62], based on the radiative transfer simulation results. However, M4 DCC reflectance is lower than M5. On the other band, NOAA-20 and S-NPP M9 DCC reflectance seems too high. The cause of the out of family VIIRS M4 and M9 DCC reflectance needs to be further investigated.

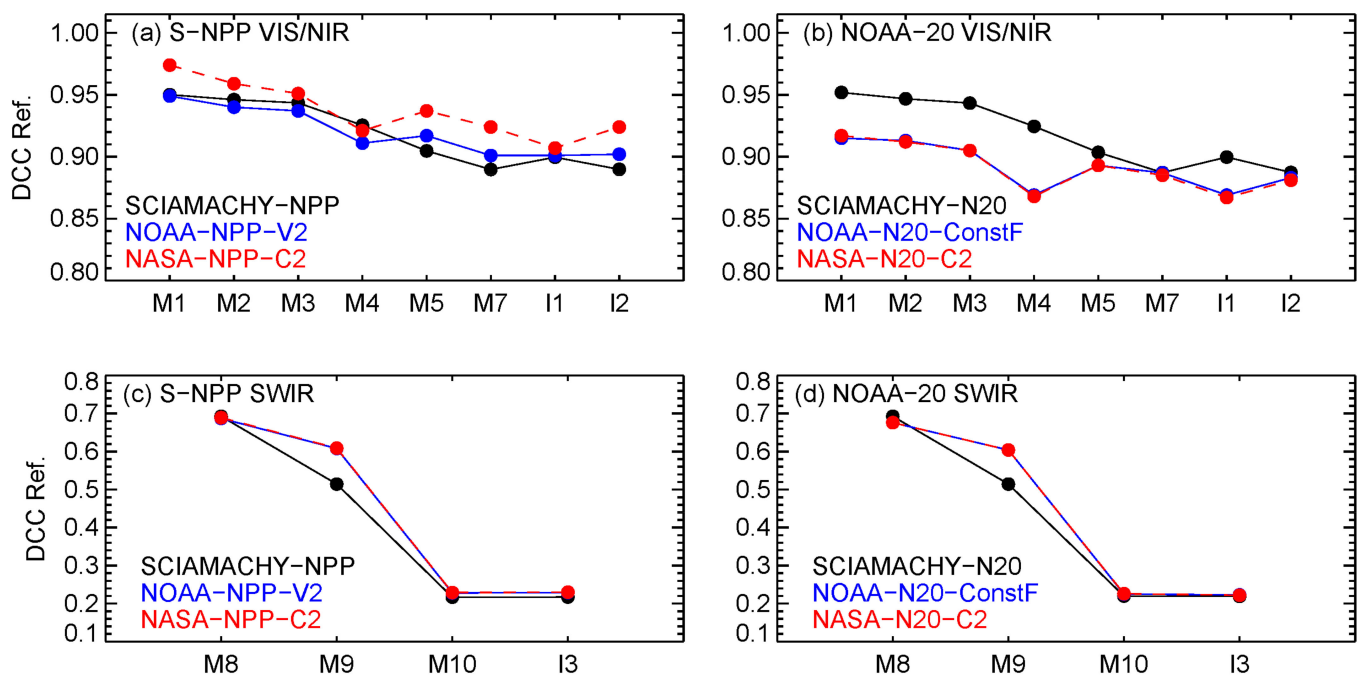


**Figure 9.** Inter-channel calibration consistency of the NOAA-20 and S-NPP RSBs: (a) S-NPP VIIRS VIS/NIR bands, (b) NOAA-20 VIIRS SWIR bands, (c) S-NPP VIIRS SWIR bands, and (d) NOAA-20 SWIR bands.

#### 4.5. Typical VIIRS RSB Radiances over DCCs

The on-orbit calibration performances of a satellite radiometer may vary slightly with the radiance levels. Figure 10 shows typical DCC radiances and ratios between typical DCC radiances and  $L_{max}$  specifications (see Table 1). For dual-gain RSBs (M1–M5 and M7),  $L_{max}$  specifications for low gain were used. Note that VIIRS-observed maximum good quality radiances are usually higher than the  $L_{max}$  specifications for the RSBs analyzed in this study. The typical DCC radiances were estimated from 10 years of S-NPP and 4 years of NOAA-20 VIIRS SDRs used in this study. The VIIRS-observed raw radiance over DCCs was used (no correction was applied). For VIS/NIR bands, typical radiances over DCCs are  $\sim 80\%$  of the  $L_{max}$  values, except for M5 and I1 ( $\sim 60\%$ ). For SWIRs, DCCs are less reflective, with typical DCC radiances of  $\sim 55\%$  of  $L_{max}$  values for M8 and  $\sim 25\%$  of  $L_{max}$  values or less for M9–M11 and I3. The DCC analysis results presented in this study may better represent the long-term calibration stability and biases at these typical DCC radiance levels.

The VIIRS long-term calibration stability and bias analysis results derived using the DCC methods are generally consistent with those derived using other vicarious methods, such as lunar calibration, PICs, and SNOs [3,52,59,63]. However, some disagreements were observed for S-NPP M3–M4 (see Section 4.1.1). The S-NPP M3–M4 results from this study may better represent the VIIRS calibration performance at high radiance levels compared to that of the lunar calibration. This topic will be further studied in the future.

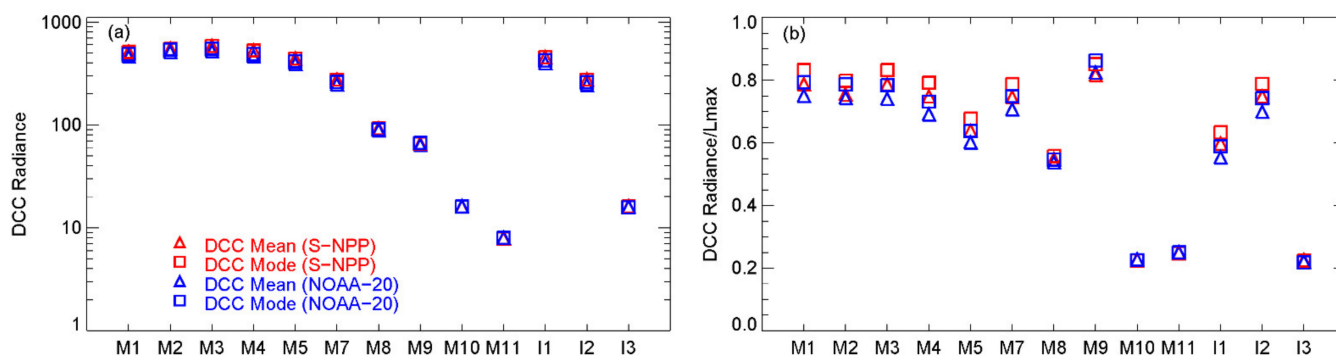


**Figure 10.** (a) Typical VIIRS RSB radiances over DCCs, and (b) ratios between typical VIIRS RSB DCC radiances and  $L_{max}$  specifications. The unit of DCC radiance is  $W/(m^2 \text{ sr } \mu\text{m})$ .

## 5. Summary

This study evaluated the long-term calibration stability, bias, and inter-channel calibration consistency of NOAA-20 and S-NPP VIIRS RSB SDRs using the DCC methods to support VIIRS RSB SDR downstream data users. Five VIIRS SDR datasets, calibrated and produced independently by the NOAA and NASA teams, were analyzed: (1) NOAA-NPP-V2 (2012–2020), (2) NASA-NPP-C1 (2012–2021), (3) NASA-NPP-C2 (2012–2021), (4) NOAA-N20-ConstF (2018–2021), and (5) NASA-N20-C2 (2018–2021).

The three S-NPP VIIRS RSB SDRs generated by the two agencies were generally stable, with trends within  $\pm 0.1\%/year$  for all bands, except for M3–M4. S-NPP M3–M4 show persistent larger trends over DCCs (0.11 to 0.17%/year) in all three data records, which are likely due to the different rates of instrument degradation in low gain and high gain in the two bands. We will further study this topic in the future. No significant trend was observed in the three NOAA-NPP-V2 bands (I2, M9, and M11); five NASA-NPP-C1 bands (M2, I1, M9–M11); and seven NASA-NPP-C2 bands (M7, I2, M8–M11, and I3). The trends in the remaining bands are significant (exceeding the 95% CIs). The calibration biases between NOAA and NASA RSB SDRs are nearly constant over time, up to 2.4% for the VIS/NIR bands and up to 0.7% for the SWIR bands.

NOAA-20 VIIRS RSB SDRs generated by NOAA and NASA are also generally stable and comparable with each other. VIS/NIR bands exhibit small downward trends, less than  $-0.08\%/year$  for NOAA-N20-ConstF and less than  $-0.13\%/year$  for NASA-N20-C2. SWIR bands show small upward trends, less than  $0.12\%/year$  for NOAA-N20-ConstF and less than  $0.16\%/year$  for NASA-N20-C2. No significant trend was observed in the NOAA-N20-ConstF RSB SDRs, except I1 (exceeding the 95% CIs). The trends in NASA-N20-C2 I1 and M2–M4 were also significant, exceeding the 95% CIs. The calibration biases between NOAA-N20-ConstF and NASA-N20-C2 were very small, within 0.2% and 0.7% for M-band and I-band RSBs, respectively.

Large inter-satellite biases exist between NOAA-20 and S-NPP VIIRS RSB SDRs, with the S-NPP RSB reflectance bias higher than NOAA-20 RSBs. The inter-satellite biases for VIS/NIR bands are larger, up to 4.5% for NOAA-generated SDRs and up to 7% for NASA-generated SDRs. The inter-satellite biases in the SWIR bands are within 0.3% for M8–M11. The biases in I3 are larger (more than 3.5%). In addition, these biases are mostly constant over time. The inter-channel calibration consistency of VIIRS RSBs was analyzed using SCIAMACHY-based DCC reflectance as the reference. The S-NPP VIIRS RSB DCC reflectance values were slightly more consistent with those of SCIAMACHY compared to NOAA-20. Bands M4 and M9 seem out of family in all five S-NPP and NOAA-20 RSB SDRs and require further investigation.

**Author Contributions:** Conceptualization, W.W.; methodology, W.W. and C.C.; software, W.W.; validation, W.W.; formal analysis, W.W.; investigation, W.W., X.S., S.B., T.C. and S.U.; resources, C.C., W.W., X.S., S.B., T.C. and S.U.; data curation, W.W., B.Z. and Y.B.; writing—original draft preparation, W.W.; writing—review and editing, W.W., C.C., B.Z., X.S., S.B., T.C., S.U. and Y.B.; visualization, W.W.; supervision, C.C.; project administration, W.W. and funding acquisition, W.W. and X.S. All authors have read and agreed to the published version of the manuscript.

**Funding:** This study was supported by NOAA grant NA19NES4320002 (Cooperative Institute for Satellite Earth System Studies—CISESS) at the University of Maryland/ESSIC.

**Data Availability Statement:** The NOAA version 2 reprocessed are available at: The data from 2012–2020 will be available from the Comprehensive Large Array-data Stewardship System (CLASS, [www.class.noaa.gov](http://www.class.noaa.gov)) in 2023. NOAA-20 VIIRS SDRs from 27 April 2018 to 31 December 2021 are available from the CLASS. The NASA S-NPP and NOAA-20 VIIRS SDRs are available from the Level-1 and Atmosphere Archive & Distribution System Distributed Active Archive Center (LAADS DAAC, <https://ladsweb.modaps.eosdis.nasa.gov/>, accessed on 1 May 2022). The reprocessed VIIRS SDRs are available on request from the corresponding author.

**Conflicts of Interest:** The authors declare no conflict of interest. The funders had no role in the design of the study; in the collection, analyses, or interpretation of the data; in the writing of the manuscript; or in the decision to publish the results.

**Disclaimer:** The scientific results and conclusions, as well as any views or opinions expressed herein, are those of the author(s) and do not necessarily reflect those of the NOAA or the Department of Commerce.

## References

1. Cao, C.; Xiong, J.; Blonski, S.; Liu, Q.; Uprety, S.; Shao, X.; Bai, Y.; Weng, F. Suomi NPP VIIRS sensor data record verification, validation, and long-term performance monitoring. *J. Geophys. Res. Atmos.* **2013**, *118*, 11664–11678. [[CrossRef](#)]
2. Cao, C.; De Luccia, F.J.; Xiong, X.; Wolfe, R.; Weng, F. Early on-orbit performance of the Visible Infrared Imaging Radiometer Suite onboard the Suomi National Polar-Orbiting Partnership (S-NPP) satellite. *IEEE Trans. Geosci. Remote Sens.* **2014**, *52*, 1142–1156. [[CrossRef](#)]
3. Choi, T.; Cao, C.; Blonski, S.; Wang, W.; Uprety, S.; Shao, X. NOAA-20 VIIRS Reflective Solar Band Postlaunch Calibration Updates Two Years In-Orbit. *IEEE Trans. Geosci. Remote Sens.* **2020**, *58*, 7633–7642. [[CrossRef](#)]
4. Wang, W.; Cao, C. Evaluation of NOAA-20 VIIRS Reflective Solar Bands Early On-Orbit Performance Using Daily Deep Convective Clouds Recent Improvements. *IEEE J. Sel. Top. Appl. Earth Obs. Remote Sens.* **2020**, *13*, 3975–3985. [[CrossRef](#)]
5. Cao, C.; Zhang, B.; Shao, X.; Wang, W.; Uprety, S.; Choi, T.; Blonski, S.; Gu, Y.; Bai, Y.; Lin, L.; et al. Mission-Long Recalibrated Science Quality Suomi NPP VIIRS Radiometric Dataset Using Advanced Algorithms for Time Series Studies. *Remote Sens.* **2021**, *13*, 1075. [[CrossRef](#)]
6. Doelling, D.; Morstad, D.; Bhatt, R.; Scarino, B. *Algorithm Theoretical Basis Document (ATBD) for Deep Convective Cloud (DCC) Technique of Calibrating GEO Sensors with Aqua-MODIS for GSICS*; World Meteorological Organization: Geneva, Switzerland, 2011.
7. Doelling, D.R.; Morstad, D.; Scarino, B.R.; Bhatt, R.; Gopalan, A. The characterization of deep convective clouds as an invariant calibration target and as a visible calibration technique. *IEEE Trans. Geosci. Remote Sens.* **2013**, *51*, 1147–1159. [[CrossRef](#)]
8. Bhatt, R.; Doelling, D.; Wu, A.; Xiong, X.; Scarino, B.; Haney, C.; Gopalan, A. Initial stability assessment of S-NPP VIIRS reflective solar band calibration using invariant desert and deep convective cloud targets. *Remote Sens.* **2014**, *6*, 2809–2826. [[CrossRef](#)]
9. Wang, W.; Cao, C. DCC radiometric sensitivity to spatial resolution, cluster size, and LWIR calibration bias based on VIIRS observations. *J. Atmos. Ocean. Technol.* **2015**, *32*, 48–60. [[CrossRef](#)]
10. Bhatt, R.; Doelling, R.D.; Scarino, B.; Haney, C.; Gopalan, A. Development of Seasonal BRDF Models to Extend the Use of Deep Convective Clouds as Invariant Targets for Satellite SWIR-Band Calibration. *Remote Sens.* **2017**, *9*, 1061. [[CrossRef](#)]
11. Wang, W.; Cao, C. Monitoring the NOAA operational VIIRS RSB and DNB calibration stability using monthly and semi-monthly deep convective clouds time series. *Remote Sens.* **2016**, *8*, 32. [[CrossRef](#)]
12. Mu, Q.; Xiong, X.; Chang, T.; Wu, A. Exploring the stability and residual response versus scan angle effects in SNPP VIIRS sensor data record reflectance products using deep convective clouds. *J. Appl. Remote Sens.* **2018**, *12*, 034006. [[CrossRef](#)]
13. Mu, Q.; Wu, A.; Xiong, X.; Angal, A. Assessment of SNPP VIIRS RSB detector-to-detector differences using deep convective clouds and deserts. *J. Appl. Remote Sens.* **2020**, *14*, 018503. [[CrossRef](#)]
14. Hu, Y.; Wielicki, B.A.; Ping, Y.; Stackhouse, P.W.; Lin, B.; Young, D.F. Application of deep convective cloud albedo observation to satellite-based study of the terrestrial atmosphere: Monitoring the stability of spaceborne measurements and assessing absorption anomaly. *IEEE Trans. Geosci. Remote Sens.* **2004**, *42*, 2594–2599.
15. Sun, J.; Wang, M. Visible Infrared Imaging Radiometer Suite solar diffuser calibration and its challenges using a solar diffuser stability monitor. *Appl. Opt.* **2014**, *53*, 8571–8584. [[CrossRef](#)]

16. Sun, J.; Wang, M. On-orbit calibration of Visible Infrared Imaging Radiometer Suite reflective solar bands and its challenges using a solar diffuser. *Appl. Opt.* **2015**, *54*, 7210–7223. [[CrossRef](#)]
17. Eplee, R.E.; Turpie, K.R.; Meister, G.; Patt, F.S.; Franz, B.A.; Bailey, S.W. On-orbit calibration of the Suomi National Polar-Orbiting Partnership Visible Infrared Imaging Radiometer Suite for ocean color applications. *Appl. Opt.* **2015**, *54*, 1984–2006. [[CrossRef](#)]
18. Sun, J.; Wang, M. Radiometric calibration of the Visible Infrared Imaging Radiometer Suite reflective solar bands with robust characterizations and hybrid calibration coefficients. *Appl. Opt.* **2015**, *54*, 9331–9342. [[CrossRef](#)]
19. Sun, J.; Wang, M. VIIRS Reflective Solar Bands Calibration Progress and Its Impact on Ocean Color Products. *Remote Sens.* **2016**, *8*, 194. [[CrossRef](#)]
20. Sun, J.; Wang, M. NOAA-20 VIIRS on-orbit calibration and characterization using the Moon. *Proc. SPIE* **2018**, *10764*, 197640.
21. Sun, J.; Chu, M.; Wang, M. On-orbit characterization of the VIIRS solar diffuser and attenuation screens for NOAA-20 using yaw measurements. *Appl. Opt.* **2018**, *57*, 6605–6619. [[CrossRef](#)]
22. Eplee, R.E.; Meister, G.; Patt, F.S.; Turpie, K.R.; Bailey, S.W.; Franz, B.A. The NASA OBPG 2020 on-orbit calibration of SNPP VIIRS for ocean color applications. *Earth Obs. Syst. XXIV* **2019**, *11127*, 254–272.
23. Sun, J.; Xiong, X.; Lei, N.; Li, S.; Twedt, K.; Angal, A. Ten Years of SNPP VIIRS Reflective Solar Bands On-Orbit Calibration and Performance. *Remote Sens.* **2021**, *13*, 2944. [[CrossRef](#)]
24. Zou, C.-Z.; Zhou, L.; Lin, L.; Sun, N.; Chen, Y.; Flynn, L.E.; Zhang, B.; Cao, C.; Iturbide-Sanchez, F.; Beck, T.; et al. The Reprocessed Suomi NPP Satellite Observations. *Remote Sens.* **2020**, *12*, 2891. [[CrossRef](#)]
25. Lei, N.; Xiong, X.; Wang, Z.; Li, S.C.; Twedt, K.A. SNPP VIIRS RSB on-orbit radiometric calibration algorithms Version 2.0 and the performances, part 2: The performances. *J. Appl. Remote Sens.* **2020**, *14*, 047502. [[CrossRef](#)]
26. Lei, N.; Xiong, X.; Wang, Z.; Li, S.C.; Twedt, K.A. SNPP VIIRS RSB on-orbit radiometric calibration algorithms Version 2.0 and the performances, part 1: The algorithms. *J. Appl. Remote Sens.* **2020**, *14*, 047501. [[CrossRef](#)]
27. Cao, C.; Wang, W. Suomi NPP/J1 VIIRS SDR Performance Highlights and Cal/Val Update. In Proceedings of the 96th American Meteorological Society Annual Meeting (Oral Presentation on Behalf of Dr. Changyong Cao), New Orleans, LA, USA, 14 January 2016.
28. Wang, W.; Cao, C. NOAA-20 VIIRS Sensor Data Records Geometric and Radiometric Calibration Performance One Year In-Orbit. In Proceedings of the 2019 International Geoscience and Remote Sensing Symposium (IGARSS), Yokohama, Japan, 28 July–3 August 2019.
29. NOAA STAR. Integrated Calibration Validation System (ICVS). Available online: <https://www.star.nesdis.noaa.gov/icvs> (accessed on 1 May 2022).
30. Thuillier, G.; Hersé, M.; Labs, D.; Foujols, T.; Peetermans, W.; Gillotay, D.; Simon, P.C.; Mandel, H. The Solar Spectral Irradiance from 200 to 2400 nm as Measured by the SOLSPEC Spectrometer from the Atlas and Eureka Missions. *Sol. Phys.* **2003**, *214*, 1–22. [[CrossRef](#)]
31. Blonski, S.; Cao, C. Suomi NPP VIIRS Reflective Solar Bands Operational Calibration Reprocessing. *Remote Sens.* **2015**, *7*, 15823. [[CrossRef](#)]
32. Choi, T.; Shao, X.; Cao, C. On-orbit radiometric calibration of Suomi NPP VIIRS reflective solar bands using the Moon and solar diffuser. *Appl. Opt.* **2018**, *57*, 9533–9542. [[CrossRef](#)]
33. Uprety, S.; Cao, C. Suomi NPP VIIRS reflective solar band on-orbit radiometric stability and accuracy assessment using desert and Antarctica Dome C sites. *Remote Sens. Environ.* **2015**, *166*, 106–115. [[CrossRef](#)]
34. Uprety, S.; Cao, C.; Blonski, S. Retrospective analysis of Suomi NPP VIIRS radiometric bias for reflective solar bands due to operational calibration changes. *Int. J. Remote Sens.* **2016**, *37*, 5472–5489. [[CrossRef](#)]
35. Shao, X.; Cao, C.; Liu, T.-C. Spectral Dependent Degradation of the Solar Diffuser on Suomi-NPP VIIRS Due to Surface Roughness-Induced Rayleigh Scattering. *Remote Sens.* **2016**, *8*, 254. [[CrossRef](#)]
36. Blonski, S. ADR 9001: Suomi NPP VIIRS Solar Calibration Anomaly on February 24, 2019H-AUTOMATE LUT Update. In Proceedings of the NOAA STAR VIIRS Radiance Team Meeting, College Park, MD, USA, 4 April 2019.
37. Zhang, B.; Cao, C.; Blonski, S.; Wang, W.; Shao, X. JPSS VIIRS Solar Vector Anomaly Root Cause Analysis and Lessons Learned. In Proceedings of the JPSS/GOES-R Proving Ground/Risk Reduction Summit, College Park, MD, USA, 24–28 February 2020.
38. Sun, J.; Xiong, X. SNPP VIIRS Reflective Solar Bands On-Orbit Calibration Using the Moon. *IEEE Trans. Geosci. Remote Sens.* **2021**, *59*, 4499–4512. [[CrossRef](#)]
39. Lei, N.; Xiong, X. Impacts of the Angular Dependence of the Solar Diffuser BRDF Degradation Factor on the SNPP VIIRS Reflective Solar Band On-Orbit Radiometric Calibration. *IEEE Trans. Geosci. Remote Sens.* **2017**, *55*, 1537–1543. [[CrossRef](#)]
40. Lei, N.; Xiong, X. Suomi NPP VIIRS Solar Diffuser BRDF Degradation Factor at Short-Wave Infrared Band Wavelengths. *IEEE Trans. Geosci. Remote Sens.* **2016**, *54*, 6212–6216. [[CrossRef](#)]
41. Lei, N.; Guenther, B.; Wang, Z.; Xiong, X. Modeling SNPP VIIRS reflective solar bands optical throughput degradation and its impacts on the relative spectral response. *Proc. SPIE* **2013**, *8866*, 461–470.
42. Lei, N.; Xiong, X.; Mu, Q.; Li, S.; Chang, T. Positional Dependence of SNPP VIIRS Solar Diffuser BRDF Change Factor: An Empirical Approach. *IEEE Trans. Geosci. Remote Sens.* **2021**, *59*, 8056–8061. [[CrossRef](#)]
43. Li, S.; Xiong, X.; Lei, N. S-NPP and N20 VIIRS RSB bands detector-to-detector calibration differences assessment using a homogeneous ground target. *Proc. SPIE* **2020**, *11501*, 357–367.

44. Sun, J.; Xiong, X. NOAA-20 VIIRS Reflective Solar bands on-Orbit Calibration Using a Hybrid Approach. In Proceedings of the 2020 IEEE International Geoscience and Remote Sensing Symposium (IGARSS), Waikoloa, HI, USA, 26 September–2 October 2020; pp. 6397–6400.
45. Sun, J.; Xiong, X. NOAA-20 VIIRS reflective solar bands on-orbit calibration. In *Sensors, Systems, and Next-Generation Satellites XXIII*; SPIE: Bellingham, WA, USA, 2019; Volume 11151.
46. Twedt, K.; Lei, N.; Xiong, X.; Angal, A.; Li, S.; Chang, T.; Sun, J. On-Orbit Calibration and Performance of NOAA-20 VIIRS Reflective Solar Bands. *IEEE Trans. Geosci. Remote Sens.* **2022**, *60*, 1–13. [[CrossRef](#)]
47. Blonski, S.; Wang, W.; Choi, T.; Shao, X.; Upreti, S.; Ahmad, K.; Gu, Y.; Zhang, B.; Bai, Y.; Cao, C. *Proposed Update of the NOAA-20 VIIRS SDR Radiometric Calibration for VisNIR Bands*; JPSS VIIRS SDR Team Telecon: College Park, MD, USA, 2021.
48. Lei, N.; Kevin, T.; Amit, A.; Sherry, L.; Tiejun, C.; Xu, G.; Xiaoxiong, X. N20 VIIRS RSB calibration algorithms and results: Collection 2.0. *Proc. SPIE* **2020**, *11501*, 233–240.
49. Lei, N.; Twedt, K.; Xiong, X. NOAA-20 VIIRS solar diffuser BRDF on-orbit change factor for wavelengths longer than 1 micron. *Proc. SPIE* **2019**, *11151*, 331–336.
50. Doelling, D.R.; Scarino, B.R.; Morstad, D.; Gopalan, A.; Bhatt, R.; Lukashin, C.; Minnis, P. The Intercalibration of Geostationary Visible Imagers Using Operational Hyperspectral SCIAMACHY Radiances. *IEEE Trans. Geosci. Remote Sens.* **2013**, *51*, 1245–1254. [[CrossRef](#)]
51. Gong, X.; Li, Z.; Li, J.; Moeller, C.C.; Wang, W. Monitoring the VIIRS Sensor Data Records Reflective Solar Band Calibrations Using DCC With Collocated CrIS Measurements. *J. Geophys. Res. Atmos.* **2019**, *124*, 8688–8706. [[CrossRef](#)]
52. Wang, W.; Cao, C.; Blonski, S.; Gu, Y.; Zhang, B.; Upreti, S.; Choi, T.; Shao, X. NOAA-20/S-NPP VIIRS Sensor Data Record On-Orbit Performance Updates and Recent Improvements. In Proceedings of the 2020 International Geoscience and Remote Sensing Symposium, Online, 26 September–2 October 2020.
53. Scarino, B.R.; Doelling, D.R.; Minnis, P.; Gopalan, A.; Chee, T.; Bhatt, R.; Lukashin, C.; Haney, C. A Web-Based Tool for Calculating Spectral Band Difference Adjustment Factors Derived From SCIAMACHY Hyperspectral Data. *IEEE Trans. Geosci. Remote Sens.* **2016**, *54*, 2529–2542. [[CrossRef](#)]
54. Bovensmann, H.; Burrows, J.P.; Buchwitz, M.; Frerick, J.; Noël, S.; Rozanov, V.V.; Chance, K.V.; Goede, A.P.H. SCIAMACHY: Mission Objectives and Measurement Modes. *J. Atmos. Sci.* **1999**, *56*, 127–150. [[CrossRef](#)]
55. Wang, W.; Cao, C.; Blonski, S.; Gu, Y.; Zhang, B.; Upreti, S. An Improved Method for VIIRS Radiance Limit Verification and Saturation Rollover Flagging. *IEEE Trans. Geosci. Remote Sens.* **2022**, *60*, 1–11. [[CrossRef](#)]
56. Xiong, X.; Angal, A.; Chang, T.; Chiang, K.; Lei, N.; Li, Y.; Sun, J.; Twedt, K.; Wu, A. MODIS and VIIRS Calibration and Characterization in Support of Producing Long-Term High-Quality Data Products. *Remote Sens.* **2020**, *12*, 3167. [[CrossRef](#)]
57. Doelling, D.; Cao, C.; Xiong, J. GSICS recommends NOAA-20 VIIRS as reflective solar band (RSB) calibration reference. *GSICS Q.* **2021**, *14*, 2–4. [[CrossRef](#)]
58. Upreti, S.; Cao, C.; Shao, X. Radiometric consistency between GOES-16 ABI and VIIRS on Suomi NPP and NOAA-20. *J. Appl. Remote Sens.* **2020**, *14*, 032407. [[CrossRef](#)]
59. Upreti, S.; Cao, C.; Blonski, S.; Shao, X. Evaluating NOAA-20 and S-NPP VIIRS Radiometric Consistency. In Proceedings of the SPIE Asia-Pacific Remote Sensing, Honolulu, HI, USA, 23 October 2018; Volume 107810. [[CrossRef](#)]
60. Moyer, D.; Upreti, S.; Wang, W.; Cao, C.; Guch, I. S-NPP/NOAA-20 VIIRS reflective solar bands on-orbit calibration bias investigation. *Proc. SPIE* **2021**, *11829*, 319–331.
61. Thompson, D.R.; McCubbin, I.; Gao, B.C.; Green, R.O.; Matthews, A.A.; Mei, F.; Meyer, K.G.; Platnick, S.; Schmid, B.; Tomlinson, J.; et al. Measuring cloud thermodynamic phase with shortwave infrared imaging spectroscopy. *J. Geophys. Res. Atmos.* **2016**, *121*, 9174–9190. [[CrossRef](#)]
62. Fougnie, B.; Bach, R. Monitoring of radiometric sensitivity changes of space sensors using deep convective clouds: Operational application to PARASOL. *IEEE Trans. Geosci. Remote Sens.* **2009**, *47*, 851–861. [[CrossRef](#)]
63. Choi, T.; Cao, C.; Shao, X.; Wang, W. S-NPP VIIRS Lunar Calibrations over 10 years in Reflective Solar Bands (RSB). *Remote Sens.* **2022**, *14*, 3367. [[CrossRef](#)]